The Plant Cell, Vol. 21: 1972–1991, July 2009, www.plantcell.org

Two Seven-Transmembrane Domain MILDEW RESISTANCE LOCUS O Proteins Cofunction in *Arabidopsis* Root Thigmomorphogenesis [C][W]

Zhongying Chen,[a,1] Sandra Noir,[b,1] Mark Kwaaitaal,[b] H. Andreas Hartmann,[b] Ming-Jing Wu,[a] Yashwanti Mudgil,[a] Poornima Sukumar,[c] Gloria Muday,[c] Ralph Panstruga,[b,2,3] and Alan M. Jones[a,d,2]

[a] Department of Biology, University of North Carolina, Chapel Hill, North Carolina 27599
[b] Department of Plant-Microbe Interactions, Max-Planck Institute for Plant Breeding Research, Cologne D-50829, Germany
[c] Department of Biology Wake Forest University, Winston-Salem, North Carolina 27109
[d] Department of Pharmacology, University of North Carolina, Chapel Hill, North Carolina 27599

Directional root expansion is governed by nutrient gradients, positive gravitropism and hydrotropism, negative phototropism and thigmotropism, as well as endogenous oscillations in the growth trajectory (circumnutation). Null mutations in phylogenetically related *Arabidopsis thaliana* genes *MILDEW RESISTANCE LOCUS O 4* (*MLO4*) and *MLO11*, encoding heptahelical, plasma membrane–localized proteins predominantly expressed in the root tip, result in aberrant root thigmomorphogenesis. *mlo4* and *mlo11* mutant plants show anisotropic, chiral root expansion manifesting as tightly curled root patterns upon contact with solid surfaces. The defect in *mlo4* and *mlo11* mutants is nonadditive and dependent on light and nutrients. Genetic epistasis experiments demonstrate that the mutant phenotype is independently modulated by the Gβ subunit of the heterotrimeric G-protein complex. Analysis of expressed chimeric MLO4/MLO2 proteins revealed that the C-terminal domain of MLO4 is necessary but not sufficient for MLO4 action in root thigmomorphogenesis. The expression of the auxin efflux carrier fusion, PIN1-green fluorescent protein, the pattern of auxin-induced gene expression, and acropetal as well as basipetal auxin transport are altered at the root tip of *mlo4* mutant seedlings. Moreover, addition of auxin transport inhibitors or the loss of EIR1/AGR1/PIN2 function abolishes root curling of *mlo4*, *mlo11*, and wild-type seedlings. These results demonstrate that the exaggerated root curling phenotypes of the *mlo4* and *mlo11* mutants depend on auxin gradients and suggest that MLO4 and MLO11 cofunction as modulators of touch-induced root tropism.

INTRODUCTION

Roots must circumnavigate barriers in soil to reach nutrient patches to optimize root growth and architecture (Osmont et al., 2007). Intense effort now focuses on engineering crop root architecture to maximize yield through improved fitness (de Dorlodot et al., 2007). Because root architecture is flexible, it also serves as a model system to study developmental plasticity, particularly toward understanding intrinsic and extrinsic factors that drive organ form (Malamy, 2005). At the molecular level, a sketch of the molecular pathway linking these signals to formation of root architecture and growth is coming into focus, but many details of these pathways remain obscure.

Root architecture develops out of a combination of cell division and expansion, lateral root formation, and cellular differentiation (e.g., root hair formation). Although roots can grow straight with lateral roots forming at regular intervals, *Arabidopsis thaliana* roots have more complex growth patterns that are environmentally sensitive. For example, root gravitropic curvature upon reorientation relative to the gravity vector is a well-characterized process (Muday and Rahman, 2007). Root waving, skewing (also termed slanting), and curling are also common growth behaviors when plants are grown on a hard surface that roots cannot penetrate (Okada and Shimura, 1990).

The major increase in root length is due to cell elongation in a zone distal to the tip. The amount and direction of growth is controlled by mechanical (touch) and gravity forces that are sensed in the root tip (Legué et al., 1997; Sack, 1997; Blancaflor et al., 1998; Fasano et al., 2001). Experimental evidence indicates that mechanical and gravity sensing are integrated to drive root growth around barriers in soil over a wide range of impedance to growth, suggesting that mechanosensing feeds back onto gravity perception or response (Massa and Gilroy, 2003a, 2003b). Mutants with altered auxin response or transport show altered gravitropism, curling, waving, and skewing responses (Okada and Shimura, 1990; Garbers et al., 1996; Luschnig et al., 1998; Rutherford et al., 1998; Marchant et al., 1999; Rashotte et al., 2001; Piconese et al., 2003; Buer and Muday, 2004), indicating a critical role for auxin in regulation of these processes. Additionally, feedback may involve the phytohormone ethylene, as this gas

[1] These authors contributed equally to this work.
[2] These authors contributed equally to this work.
[3] Address correspondence to panstrug@mpiz-koeln.mpg.de.
The authors responsible for distribution of materials integral to the findings presented in this article in accordance with the policy described in the Instructions for Authors (www.plantcell.org) are: Ralph Panstruga (panstrug@mpiz-koeln.mpg.de) and Alan M. Jones (alan_jones@unc.edu).
[C]Some figures in this article are displayed in color online but in black and white in the print edition.
[W]Online version contains Web-only data.
www.plantcell.org/cgi/doi/10.1105/tpc.108.062653

inhibits root waving (Buer et al., 2003), root gravitropism (Buer et al., 2006), and lateral root formation (Negi et al., 2008).

Thigmomorphogenesis is defined as the sum of growth responses of a plant organ in response to a mechanical stimulus (Jaffe et al., 2002). The molecular basis of the touch sensors and signal transduction components that finally give rise to differential organ growth is largely unknown. It is thought that Ca^{2+} plays a key role as a second messenger in signal transduction during mechanosensing (e.g., via the activation of mechanosensitive Ca^{2+} channels) (Jaffe et al., 2002). Indeed, rapid and transient changes in the concentration of cytosolic free Ca^{2+} levels (Ca^{2+} spikes) were observed upon mechanical stimulation in roots (Knight et al., 1991; Legué et al., 1997). Cloning of a set of touch-induced genes, of which three encode either calmodulin or calmodulin-related proteins, and identification of a plasma membrane protein that links mechanosensing with Ca^{2+} influx provides genetic evidence for the importance of Ca^{2+} signaling in this physiological process (Braam and Davis, 1990; Sistrunk et al., 1994; Nakagawa et al., 2007a).

Some mechanosensing pathways in human cells and fungi involve cell surface seven-transmembrane (7TM) domain receptors coupled to heterotrimeric G-proteins that activate phospholipase C, leading to rapid transient calcium increases in the cytoplasm (Chachisvilis et al., 2006; Kumamoto, 2008). *Arabidopsis* encodes a limited number of predicted 7TM domain proteins (Moriyama et al., 2006; Gookin et al., 2008), and within this set, the largest protein family consists of 15 members. They are designated Mildew Resistance Locus O (MLO) since genetic studies revealed that several of these proteins, including the earliest identified barley (*Hordeum vulgare*) MLO and its co-orthologs, MLO2, MLO6, and MLO12 in *Arabidopsis*, function in modulating antifungal defense, possibly through negatively regulating cell death and senescence-related physiology (Büschges et al., 1997; Piffanelli et al., 2002; Consonni et al., 2006). Although MLO proteins are plant specific at the level of amino acid sequences, structural features of these proteins are similar to those of metazoan G-protein-coupled receptors (GPCRs). MLOs are plasma membrane delimited via their 7TM domains with the N terminus positioned extracellularly and the C terminus intracellularly (Devoto et al., 1999). Potential in planta homodimerization of MLO proteins has been revealed by Förster/fluorescence resonance energy transfer analysis (Elliott et al., 2005).

Here, we used a reverse genetics approach to identify 7TM domain proteins that play a role in root-associated physiological processes. We discovered two *MLO* genes, *MLO4* and *MLO11*, that cofunction in root thigmomorphogenesis. By employing a combination of genetic epistasis analysis, chemical genetics, and cell biology, we demonstrate that the touch-induced anisotropic root growth in *mlo4* and *mlo11* mutants is auxin dependent. We propose that MLO4 and MLO11 operate in a heterooligomeric complex to regulate thigmotropic root growth.

RESULTS

MLO4 and MLO11 Modulate Asymmetrical Root Growth

We isolated and characterized T-DNA insertion lines of all genes in the 15-member *Arabidopsis MLO* family, including at least two independent alleles each for *MLO4* (*mlo4*-1, *mlo4*-3, and *mlo4*-4), *MLO11* (*mlo11*-3 and *mlo11*-4), and *MLO14* (*mlo14*-6 and *mlo14*-7), the subjects of this study (Figure 1A). As assayed by RT-PCR, these *mlo4*, *mlo11*, and *mlo14* mutant plants lacked detectable full-length transcripts of the respective *MLO* genes, suggesting that all are null mutant alleles (see Supplemental Figure 1 online; *mlo4*-3 not tested). *MLO4*, *MLO11*, and *MLO14* are the sole members of a defined phylogenetic clade within the *Arabidopsis MLO* family (Devoto et al., 2003; Chen et al., 2006) and have unknown functions. Prominent expression of *MLO4*, *MLO11*, and *MLO14* in the root tip (Chen et al., 2006) prompted us to investigate root-related growth phenotypes in the respective mutants. In the context of these experiments, we discovered asymmetrical root growth patterns of *mlo4* and *mlo11* mutants on horizontal surfaces.

Under the conditions used here (minimal medium; see Methods), wild-type roots grew either in a less-consistent growth trajectory, comprising a combination of straight and undulating growth, or in a moderate coiling pattern, also known as root curling (Mirza, 1987). Penetrance of one or the other root growth type was shown to be subject to natural genetic variation (see Supplemental Figure 2A online) and also dependent on various exogenous parameters, such as medium composition and hardness (Buer et al., 2000). Recessive *mlo4* and *mlo11* alleles, but not *mlo14* alleles, exhibited exaggerated root curvature typically resulting in a tight spiral-like root growth pattern that exaggerates the mild root bending of the parental Columbia-0 (Col-0) wild-type plants (Figure 1B). These root coils were qualitatively distinct from the natural repertoire of root curling observed in a range of *Arabidopsis* ecotypes that are part of a core set representing accessions with maximal genetic and morphological diversity (see Supplemental Figure 2A online; McKhann et al., 2004). Root coiling of *mlo4* and *mlo11* mutants was robust on minimal media with varying sucrose content and agar source (see Supplemental Figure 2B online) but was less prominent on medium containing Murashige and Skoog (MS) salts, indicating that one or more ingredient(s) of the MS salts interfere(s) with this phenotype. Formation of *mlo4* and *mlo11* root coils is not triggered spontaneously but requires a tactile stimulus (e.g., contact of the root tip with a hard surface) (Figure 1C), suggesting that *mlo4* and *mlo11* mutants might be defective in thigmomorphogenesis. Besides aberrant root curling, *mlo4* mutant seedlings and to a lesser degree also *mlo11* seedlings, but not *mlo14* seedlings, exhibited irregular root-waving patterns on tilted hard agar containing minimal medium. This phenotype included shorter wavelengths, resulting in compressed root growth tracks (*mlo4*), and apparently stochastic formation of loops (*mlo4* and *mlo11*; Figure 1D). Moreover, root slanting on inclined hard surfaces was also altered in case of the *mlo4* mutant. Compared with the Col-0 wild-type control, which showed the previously reported right-handed (to the left when viewed from the top; Migliaccio et al., 2009) skewing pattern, *mlo4* mutants showed less root skewing but exhibited a more prominent waving growth pattern. By contrast, the degree of skewing for *mlo11* and *mlo14* was indistinguishable from the wild type (Figure 1E).

Although the qualitative differences in root growth patterns between genotypes were visibly evident, we sought to quantify root curling and skewing of *mlo4* and *mlo11* mutants. In the case

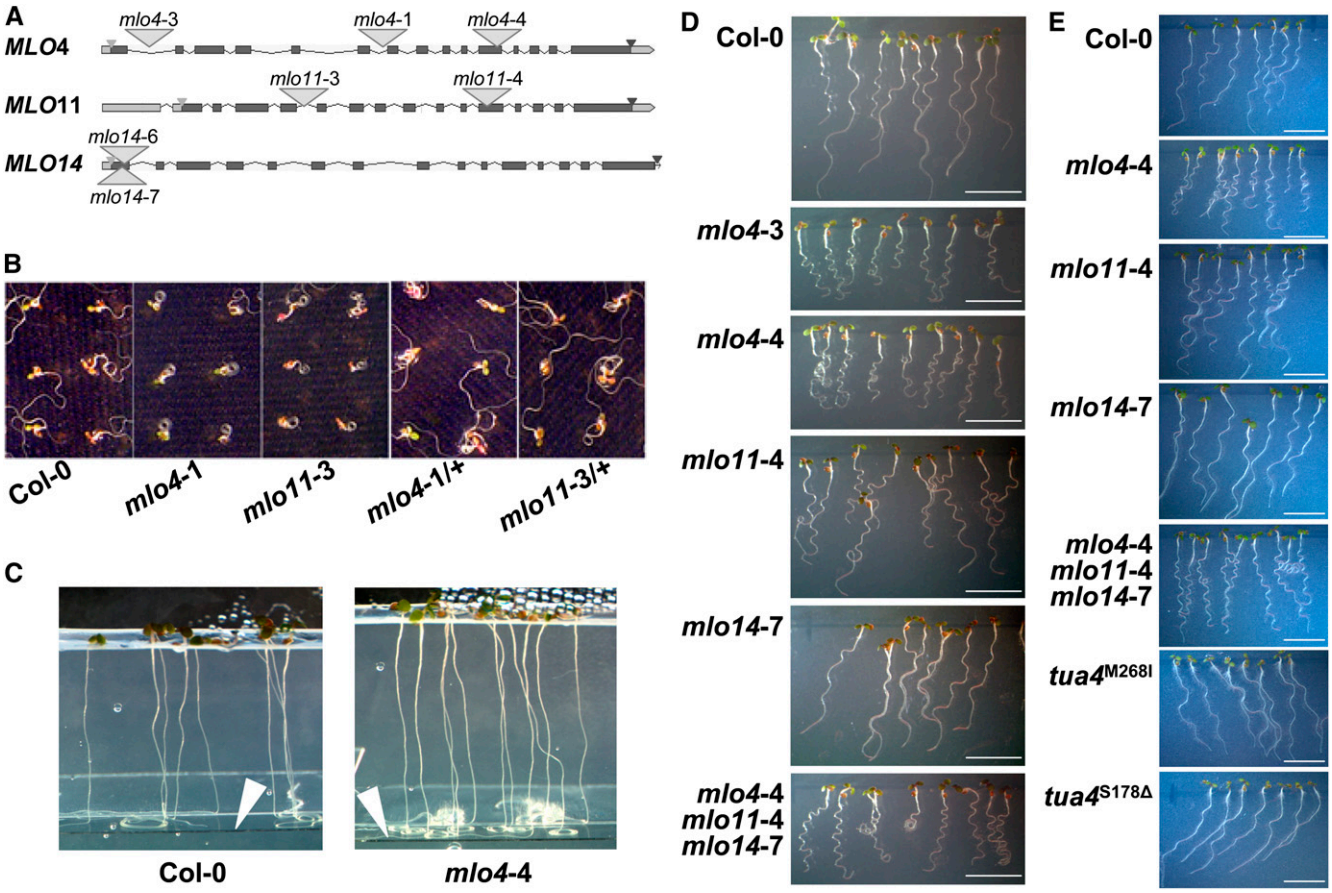

Figure 1. MLO4 and MLO11 Cofunction in Regulating Asymmetrical Root Growth.

(A) Genetic map of the T-DNA insertion alleles of *mlo4*, *mlo11*, and *mlo14* mutants used in this study. *MLO* exons are represented by dark-gray rectangles and introns by connecting lines; the arrowhead at the end of the last exon indicates 5′–3′ directionality of the genes. Sites of T-DNA insertion in the various mutant alleles are marked by light-gray triangles. Smaller light- and dark-gray triangles denote the location of translational start and stop codons, respectively.

(B) Altered root growth of *mlo4* and *mlo11* mutants on horizontal plates (minimal medium, 1% sucrose) viewed from the bottom. Seedlings of indicated genotypes were grown under continuous light for 5 d before taking pictures.

(C) A tactile stimulus triggers *mlo4*-mediated root spirals. Col-0 and *mlo4*-4 seedlings were grown vertically on minimal medium (0.25% sucrose) for 5 d (12-h light/dark cycle) when a glass cover slide (white arrowhead) was positioned a few millimeters under the root tip. Root growth patterns on the cover slide were observed 4 d later. Note the mild coiling or undulating growth of Col-0 roots compared with the tight curls of *mlo4* roots.

(D) and **(E)** Root waving **(D)** and skewing **(E)** phenotypes of *mlo* mutant seedlings. Seedlings were vertically grown on hard minimal medium (0.25% sucrose) for 2 d (12-h light/dark cycle); then, plates were slanted at 45° or 35° for observation of waving or skewing phenotypes, respectively. Photographs were taken 4 d later from the top of the agar plate. Mutants *tua4*^{M268I} and *tua4*$^{S178\Delta}$, showing either left-handed (to the right when viewed from the top) or exaggerated right-handed slanting, respectively, were included as controls for aberrant skewing phenotypes (Ishida et al., 2007). Bars = 5 mm.

of root curling, two methods were used and the results from both methods concurred (see Supplemental Figure 3 online). One procedure, first described by Mirza (1987), provides the total root angle, which is positively correlated with curling. Typically, this method reports the general direction of curling (handedness relative to the gravity vector). The second approach captures the largest span of the root coil or trajectory, which is negatively correlated to the degree of root curling. We modified the Mirza method by normalizing against root length to eliminate differences due to growth rate and compared it to the root span method to show that both methods adequately quantitated this type of anisotropic growth pattern (see Supplemental Figure 3 online). As shown in Figures 2A and 2B, curling of *mlo4* and *mlo11* roots was greater than the wild type, whereas disruption of *MLO14* alone had no effect on root curling. Root curling of *mlo4* mutants occurred more consistently and frequently in tighter spirals than in *mlo11* seedlings, which was apparent by the statistically significant difference in variance between the *mlo4* and *mlo11* mutants (Figure 2A). Quantitative analysis also corroborated sucrose independence of *mlo4*-conditioned root

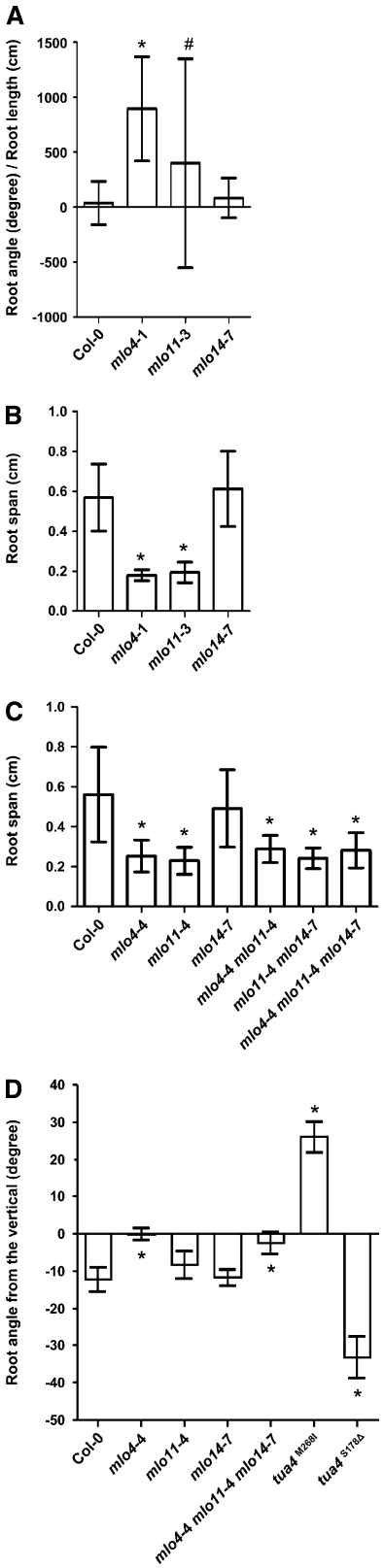

Figure 2. Quantification of Root Coiling in *mlo4* and *mlo11* Mutant Seedlings.

curling (see Supplemental Figure 2C online). Quantification of skewing indicated that the *mlo4* roots skewed significantly less than wild-type roots (Figure 2D).

The fact that disruption of either *MLO4* or *MLO11* is sufficient to cause detectable alterations in touch-induced asymmetrical root growth supports cofunction of the two genes rather than redundancy. Since *mlo4* and *mlo11* exhibited subtle yet consistent differences in their exaggerated asymmetrical root growth patterns (Figure 2A), MLO4 and MLO11 may regulate the same process(es), but each protein might play slightly different roles. The *mlo4 mlo11* double mutant and the *mlo4 mlo11 mlo14* triple mutant did not show an additional reduction in root span (Figure 2C) or further exaggeration of aberrant root waving or skewing patterns (Figures 1D, 1E, and 2D), further supporting cofunctionality of the MLO4 and MLO11 polypeptides. Alternatively, the extent of root curling may have a limit for a root of a given length.

mlo4 Mutants Exhibit Unaltered Root Architecture and Gravitropic Responses

To obtain insight into the potential mechanism of *mlo4*-conditioned root curling, we studied the morphology of *mlo4* and *mlo11* mutants in comparison to roots of wild-type plants. Our analyses revealed no obvious difference with respect to size, number, and organization of characteristic cell files of the root tip (see Supplemental Figure 4A online). Additionally, spiral roots of *mlo4* and *mlo11* mutants did not exhibit twisted epidermal cell

(A) Accumulated end-point curvature of 5-d-old light-grown seedling roots on horizontal plates (minimal medium, 1% sucrose). Positive numbers represent counterclockwise coils (as viewed from the bottom) and depict right-handed growth. Negative numbers represent clockwise root curvatures.

(B) Seedling root span (the distance from the root tip to the root base) on horizontal plates (minimal medium, 1% sucrose). Data for **(A)** and **(B)** were collected from the same 5-d-old light-grown sample population.

(C) Root span of 5-d-old, light-grown seedlings on horizontal plates (minimal medium, 1% sucrose). For each experiment in **(A)** to **(C)**, at least 25 samples were measured per genotype. Shown are data from one replicate each; all experiments were repeated at least once yielding similar results. Columns indicate the average, and error bars represent SD. Asterisks indicate a statistically significant ($P < 0.05$) difference in comparison to Col-0 according to Bonferroni's multiple comparison test, the # symbol indicates statistically significantly different ($P < 0.01$) variances between the *mlo4*-1 and *mlo11*-3 data sets according to an F-test. Please note that the latter differs from the statistically nonsignificant variances between the *mlo4*-1 and *mlo-11*-3 data sets of dark-grown seedlings shown in Figure 4E.

(D) Quantification of root skewing phenotypes from seedlings vertically grown on hard minimal medium (0.25% sucrose) as described in Methods. Root slanting angles were measured from the vertical; right-handedness (to the left when viewed from the top; cf. Figure 1D) was scored as negative and left-handedness as positive angle. Columns indicate the mean, and error bars the SD based on three replicates. For each replicate, 12 to 19 samples were measured per genotype. Asterisks indicate a statistically significant ($P < 0.05$) difference in comparison to Col-0 according to Bonferroni's multiple comparison test.

files, excluding touch-triggered organ torsion as a possible cause for the root curling phenomenon (see Supplemental Figure 4B online). To unravel potential alterations in molecular root architecture, we crossed transgenic lines expressing fluorescent marker proteins (*pPIN1:PIN1*-green fluorescent protein [*GFP*], *pPIN2:PIN2-GFP*, and *pSCR:GFP*) for root cell identity with the *mlo4*-1 or *mlo4*-3 mutant. Roots of F2 progeny of these crosses that were homozygous for *mlo4* and expressed the respective fluorescent marker protein were either grown vertically (straight roots) or horizontally (curling roots in case of *mlo4*) and imaged by confocal microscopy. Micrographs revealed similar cellular distribution patterns for the tested polypeptides in both conditions. However, there were potential differences in expression levels and/or protein turnover rates that in part depended on the growth mode. Compared with the wild-type background, PIN1-GFP levels were reduced in the vascular bundle, the pericycle, and the endodermis in horizontally but not in vertically grown roots of the *mlo4* mutant (Figure 3). By contrast, PIN2-GFP levels were higher in the *mlo4* mutant background in both growth conditions (Figure 3A; see Supplemental Figure 5 online). The latter may either be a consequence of the *mlo4* mutation or represent the result of variation in transgene expression, thus precluding firm conclusions. In both genotypes (the wild type and *mlo4* mutant), GFP fluorescence patterns originating from the *pSCR:GFP* transgene were too variable and patchy to allow reliable quantification. In sum, these findings indicate that the overall root architecture is unaltered in *mlo4* mutants, while steady state levels of the root cell marker PIN1 are conditionally affected in *mlo4* roots.

We analyzed root gravitropic responses in *mlo4* and *mlo11* single mutants and the *mlo4 mlo11* double mutant in comparison to wild-type plants to test the hypothesis that lesions in graviperception or graviresponsiveness caused the root behavior phenotypes of the *mlo4* and *mlo11* mutants. The kinetics of gravity-induced root bending of light-grown seedlings on minimal medium were similar in Col-0, *mlo4*-3, *mlo4*-4, *mlo11*-3, *mlo11*-4, and *mlo4*-4 *mlo11*-4 (see Supplemental Figure 6 online), indicating that *mlo4* and *mlo11* mutants are not defective in root gravitropism under these growth conditions. Consistent with this finding, the amount and positioning of starch-containing statoliths in *mlo4* and *mlo11* mutants were indistinguishable from the wild type (data not shown). Taken together, these data suggest that the altered root growth pattern of *mlo4* and *mlo11* mutants is not a consequence of globally perturbed root architecture or major defects in graviperception/gravitropism.

Phenotypes of *mlo4* and *mlo11* Mutants Are Light Dependent

Environmental factors, such as light and gravity, affect the mild root curling of wild-type plants (Mirza, 1987). We observed that *Arabidopsis* mutants defective in responding to gravity did not show the wild-type level of root curling under darkness (Figures 4A and 4B). This applied to *phosphoglycerate mutase1* (*pgm1*-1) and *ADP glucose phosphorylase 1* (*adg1*-1), two mutants with reduced starch biosynthesis. By contrast, the *multidrug resistance protein1/ATP binding cassette transporter b19* (*mdr1*-100/*abcb19*) mutant, which is defective in an auxin efflux transporter

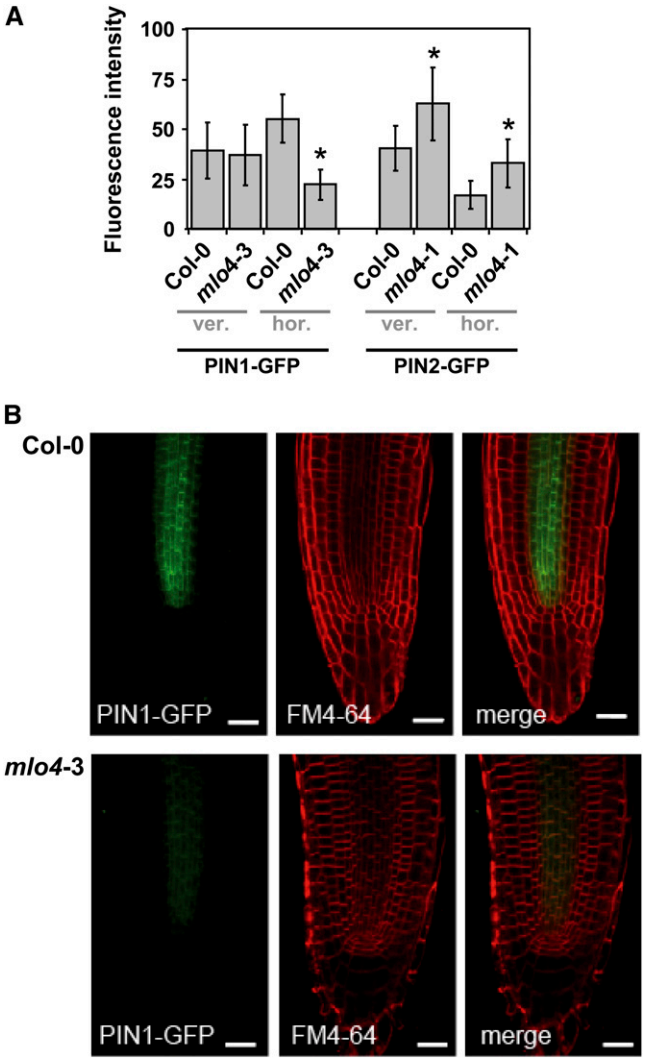

Figure 3. Roots of *mlo4* Mutants Exhibit Growth-Dependent Differences in the Accumulation of the Cell Identity Marker PIN1.

(A) Comparison of average GFP fluorescence intensities in projections of z-stacks through the root for tested reporter constructs in Col-0 and *mlo4* mutant primary roots. Seedlings were grown for 6 d (12-h light/dark cycle) either horizontally (hor.) or vertically (ver.) on minimal medium (0.25% sucrose). The bar graph depicts mean fluorescence intensities (±SD) based on ~10 root tips per genotype and growth condition. The asterisks indicate a statistically significant ($P < 0.01$) difference in comparison of GFP signal intensities in *mlo4* primary root tips to those in Col-0 primary root tips according to two-tailed Student's *t* test with unequal variances. Shown are data from one replicate; the experiment was repeated once, yielding similar results.

(B) Representative fluorescence micrographs of horizontally grown, 6-d-old Col-0 and *mlo4-3* seedlings expressing PIN1-GFP under the control of its own promoter. The micrographs show the GFP and FM4-64 fluorescence, respectively, and a merged image of both channels in an optical z-section at the level of the quiescent center of the primary root tips. Seedlings were grown horizontally (minimal medium, 0.25% sucrose; 12-h light/dark cycle) and stained for 10 min with FM4-64. Bars = 20 μm.

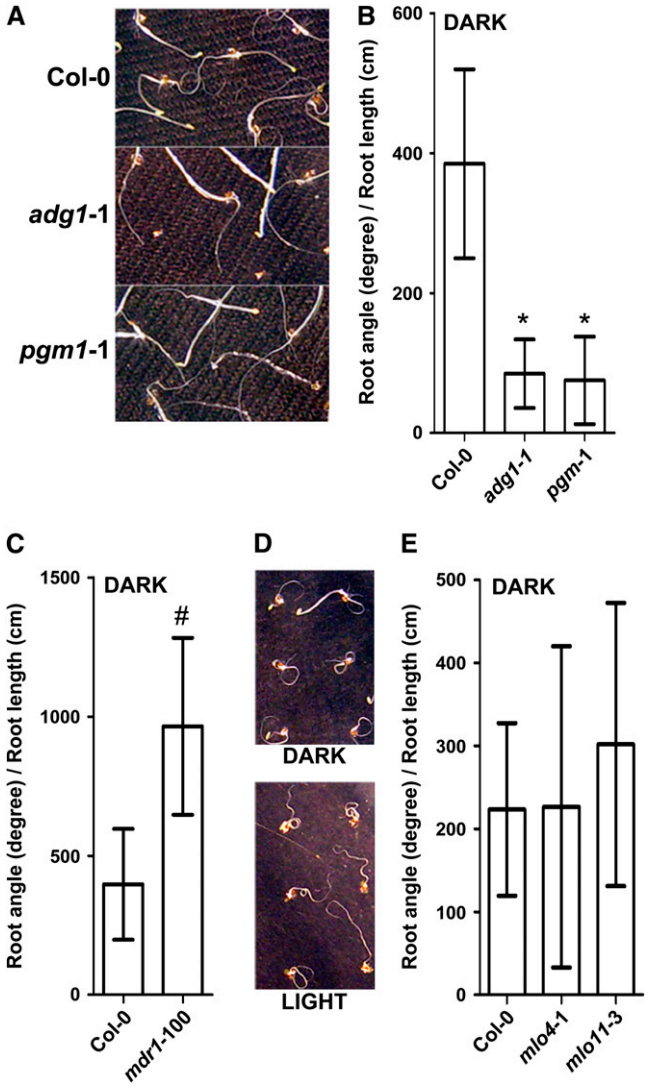

Figure 4. Root Curling Phenotypes of *mlo4* and *mlo11* Mutants Are Light Dependent.

(A) and **(B)** Horizontal root curvature of *Arabidopsis* mutants defective in responding to gravity. Seedling roots of the wild type, *pgm1*-1, and *adg1*-1 were grown on minimal medium (1% sucrose) under darkness for 5 d before recording the image from the bottom **(A)** and measuring accumulated end-point root curvature **(B)**.

(C) Accumulated end-point root curvature of 5-d-old, dark-grown *mdr1*-100 mutants viewed from the bottom.

(D) Comparison of light- and dark-grown wild-type (Col-0) seedling roots. Seedlings were grown on horizontal plates (minimal medium, 1% sucrose) for 5 d either in darkness or under constant low light (25 μM m^{-2} s^{-1}) from above. Digital images were captured from the plate bottom.

(E) Accumulated end-point root curvature of 5-d-old, dark-grown (minimal medium, 1% sucrose) wild-type, *mlo4*-1, and *mlo11*-3 seedlings. Columns indicate the mean, and error bars represent SD. At least 15 samples were measured for each genotype. Shown are data from one replicate each; all experiments were repeated at least once, yielding similar results. Asterisks indicate a statistically significant ($P < 0.05$) difference in comparison to Col-0 according to Bonferroni's multiple comparison test; the # symbol indicates a statistically significant ($P < 0.05$) difference in comparison to Col-0 according to Student's *t* test. The variance (according to an F-test) between the *mlo4*-1 and *mlo-11*-3 data sets of dark-grown seedlings shown is not significant (Figure 4E) in contrast with the variance observed with light-grown seedlings (Figure 2A). [See online article for color version of this figure.]

and shows enhanced gravitropic and/or waving responses (Lin and Wang, 2005; Lewis et al., 2007), curled more tightly under darkness than Col-0 wild-type roots (Figure 4C).

Light affects the magnitude of curling and the associated variance in the root populations of Col-0, *mlo4*-1, and *mlo11*-3. Under the conditions used here, roots of Col-0 wild-type plants curled more in darkness than in light (cf. Figures 4D and 2A to 4E). *mlo4*- and *mlo11*-conditioned root curling was significantly greater than the wild type both under constant light of weak intensity (30 μmol m^{-2} s^{-1}) and in 12-h light/dark cycles of higher light intensity (100 μmol m^{-2} s^{-1}). However, for dark-grown roots, differences in curling magnitude were not observed between the wild type and the *mlo4*-1 and *mlo11*-3 mutants (Figure 4E). The fact that the abnormal root curling pattern of the *mlo4* and *mlo11* mutants is light dependent suggests that the phenotype of these mutants may be associated with a defect in either perceiving or responding to a light-associated or photosynthesis-derived signal.

MLO4 and the Heterotrimeric G-Protein Complex Operate on Different Pathways in Regulating Asymmetrical Root Growth

Since the 7TM domain topology of MLO proteins resembles metazoan/fungal GPCRs, they are candidate plant GPCRs (Devoto et al., 1999; Kim et al., 2002; Moriyama et al., 2006). Therefore, we performed epistasis analysis between *mlo4* alleles and null mutations in heterotrimeric G-protein subunit genes. *Arabidopsis GPA1* and *AGB1* genes encoding α- and β-subunits of the G-protein complex (Temple and Jones, 2007), respectively, are expressed in root tips (Chen et al., 2006). Roots of the *agb1*-2 mutant curled less than the wild type (Figure 5), suggesting an involvement of AGB1 in modulating asymmetrical root growth. Assuming that at least some of the mechanism underlying root waving is shared by root curling, a concept that is supported by previous studies (Simmons et al., 1995) and our own data (Figures 1B and 1D), it is worth noting that *agb1*-2 mutant roots also showed reduced root waving (Pandey et al., 2008). Roots of the *agb1*-2 *mlo4*-1 double mutant curled less than those of the *mlo4*-1 single mutant but more than those of the *agb1*-2 mutant, although this difference was not statistically significant (Figure 5). These data suggest that the combination of these two mutant alleles is phenotypically additive rather than one mutant allele being clearly epistatic to the other. By contrast, the *gpa1*-4 mutation had less impact, if any, on root curling (Figure 5), which is consistent with its wild-type-like root waving phenotype (Pandey et al., 2008). These findings demonstrate that AGB1, but not GPA1, plays a role in both root curling and waving. The data also show that the effect of the null *agb1* mutation does not depend on a functional MLO4 and vice versa,

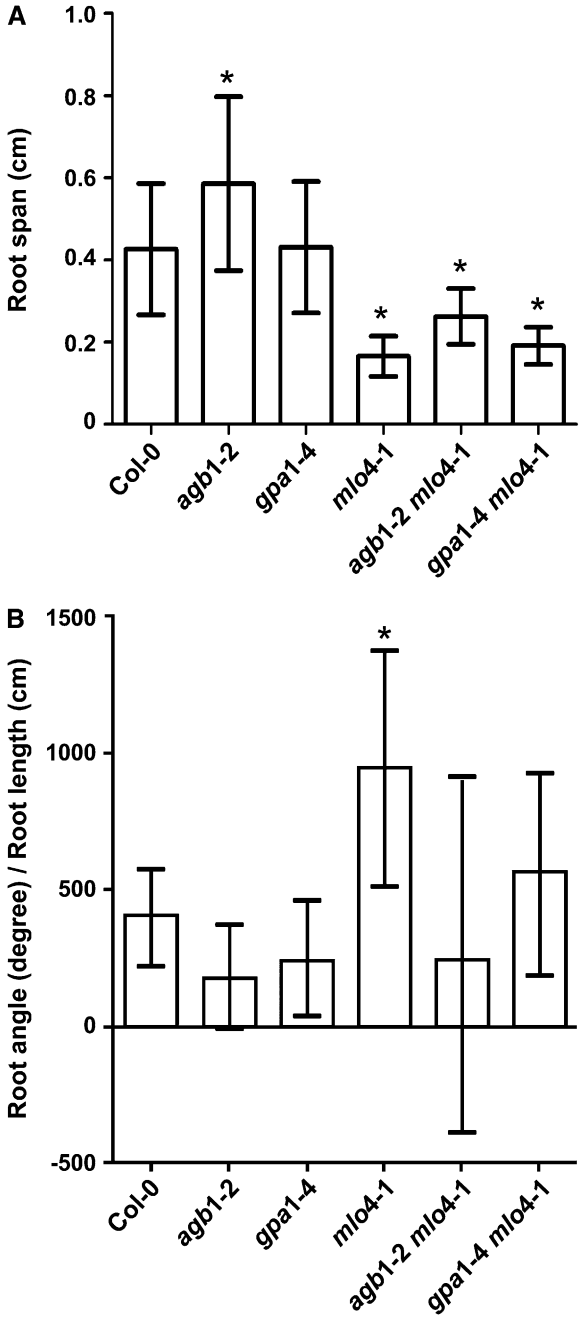

Figure 5. Epistasis Analysis on *mlo4* and G-Protein Mutants.

Seedling root span **(A)** and accumulated end-point curvature **(B)** of *mlo4*-1, G-protein mutants *gpa1*-4 and *agb1*-2, and their double mutants. Columns indicate the average, and the error bars represent SD. More than 25 seedlings were measured for each genotype. Seedlings were grown on horizontal plates (minimal medium, 1% sucrose) under constant light for 5 d. Shown are data from one exemplary replicate; the experiment was repeated once, yielding similar results. Asterisks indicate a statistically significant ($P < 0.05$) difference in comparison to Col-0 according to Bonferroni's multiple comparison test.

suggesting that the MLO4 activity in root growth patterning is independent of the heterotrimeric G-protein complex.

The C-Terminal Cytoplasmic Domain of MLO4 Is Necessary but Not Sufficient for Regulation of Asymmetrical Root Growth

Swapping domains between sequence-related proteins of two different known signaling pathways is a powerful way to map protein function to structure. To identify functional domains of MLO4, we swapped domains between MLO4 and MLO2, two MLO proteins that function in distinct physiological processes. Whereas members of the phylogenetic branch comprising MLO4, MLO11, and MLO14 are involved in regulating asymmetrical root growth, members of the clade comprising MLO2, MLO6, and MLO12 play a role in modulating antifungal defense in leaf epidermal cells (Consonni et al., 2006). Although *MLO4* and *MLO11* are expressed in leaf tissues (Chen et al., 2006), *mlo4* and *mlo11* T-DNA insertion mutants retain the wild-type level of susceptibility to fungal (powdery mildew) infections (Consonni et al., 2006). Similarly, although *MLO2*, the gene with the major modulatory role in antifungal defense, is expressed in roots (Chen et al., 2006), a powdery mildew resistant *mlo2* T-DNA insertion mutant displayed wild-type root growth patterns (see Supplemental Figure 7 online).

Functional specificity of MLO paralogs may reside in amino acid sequences of these proteins that are evolutionarily conserved within each phylogenetic clade (Panstruga, 2005). To elucidate this possibility, we focused on the regions that we identified to be of greatest dissimilarity between MLO2 and MLO4: the first extracellular loop (e1) and the cytoplasmic C terminus (c4). To perform domain swaps between these domains, we dissected the MLO proteins into four segments: the N-terminal fragment before the e1 loop, the e1 loop, the central region between e1 and c4, and the C-terminal c4 fragment. We created binary vectors harboring synthetic genes designed to express all 16 possible combinations of MLO2-MLO4 chimeras (Figure 6) as fusion with a C-terminal GFP tag to monitor protein expression levels and subcellular localization in the transgenic lines. Expression of the chimeric genes was under the control of the native *MLO4* promoter (represented by a 1.05-kb DNA fragment covering the 5′ upstream region of *MLO4* before the start codon; see Methods). All constructs were transformed into the *mlo4*-1 null mutant background to assess complementation of the *mlo4* root curling phenotype by the chimeric MLO fusion proteins.

Progeny (T2 seedlings) of six independent transgenic lines for each construct were analyzed. All lines yielded detectable GFP signals in the root tip region, although the expression levels and subcellular localization patterns varied between constructs and between transgenic lines (see Supplemental Figure 8 online). Full-length *MLO4* cDNA, but not the full-length *MLO2* cDNA, rescued the *mlo4* root curling phenotype (Figures 6A and 6B; for definition of criteria for complementation, see Methods). MLO4 harboring the e1 loop or the N terminus plus the e1 loop from MLO2 also complemented the *mlo4* mutant phenotype (Figures 6E and 6K), suggesting that these MLO2-derived domains are either functionally equivalent to the respective MLO4 regions or

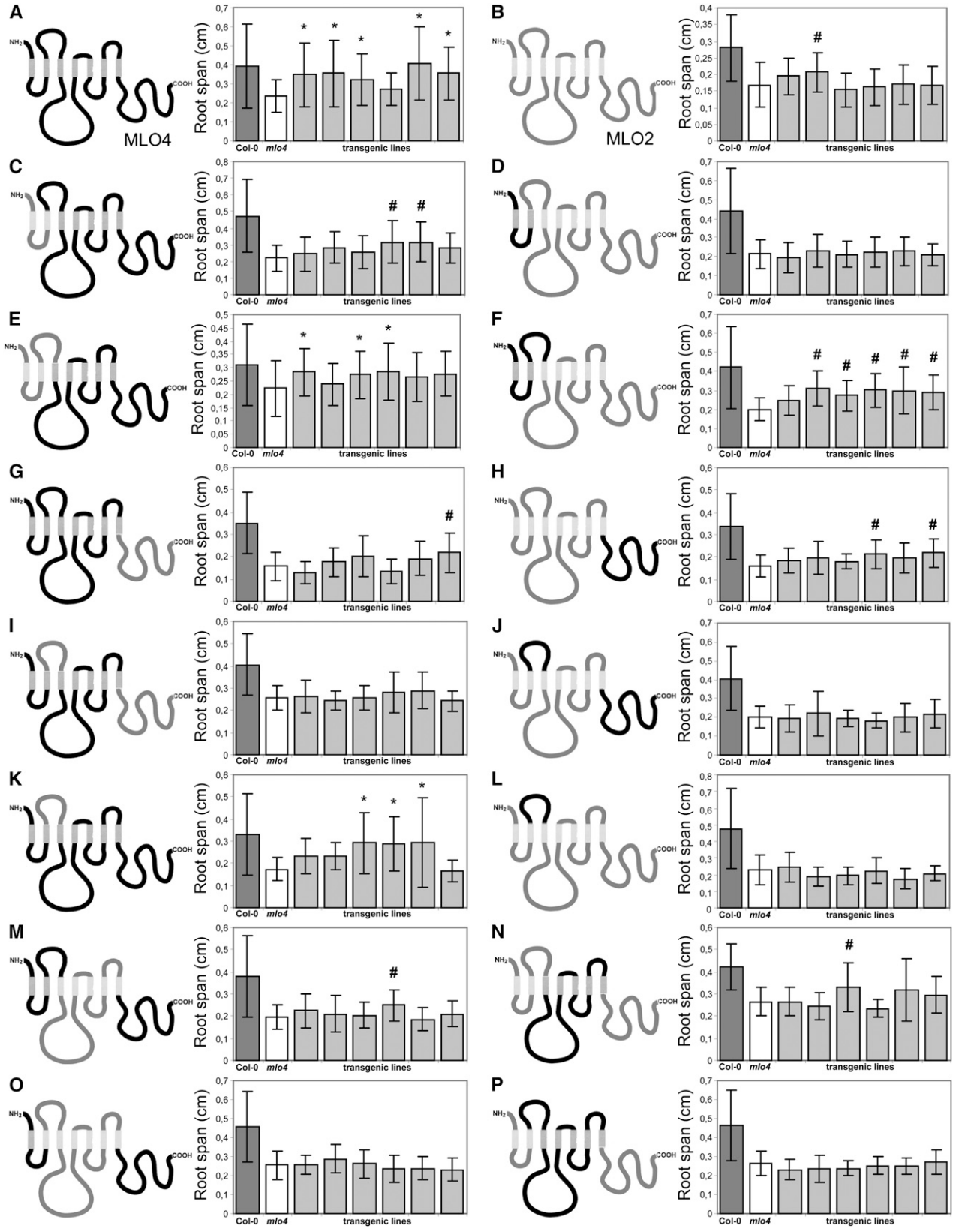

Figure 6. Structure-Function Analysis of MLO4.

that the identity of these parts of the protein is subordinate for MLO4 function. By contrast, an MLO4 chimera with the MLO2 c4 domain did not complement (Figure 6G), indicating the importance of the identity of this domain for functional specificity. Since MLO2 with c4 from MLO4 partially complemented the mutant phenotype (Figure 6H), functional specificity of MLO proteins seems to require the coordinated action of multiple cytoplasmic domains (Elliott et al., 2005). This hypothesis is further supported by the fact that all other chimeric proteins, with one exception that permitted partial complementation (Figure 6F), failed to rescue the *mlo4* root curling phenotype. Given the variance of this assay, it remains possible that we underestimated the capacity of some chimeric proteins for complementation owing to differential expression, stability, or ectopic subcellular localization of the respective artificial polypeptides.

mlo4-Conditioned Root Curling Requires Normal Auxin Transport

An unbiased chemical genetic screen of 2300 tested substances from three compound libraries (for details, see Methods) yielded 14 low molecular weight compounds that attenuated the exaggerated root curling phenotype of *mlo4* and *mlo11* mutants in a dosage-dependent manner (see Supplemental Figure 9 online). Among these 14 compounds were the auxin transport inhibitors 1-*N*-naphthylphthalamic acid (NPA), difluenzopyr and quinchlorac, the vesicle transport inhibitor Brefeldin A (BFA), four benzopyrans (methylesculetin, karanjin, robustic acid, and prunetin), and six structurally related compounds of unknown chemical identity (see Supplemental Figure 9B online). Three of the four detected benzopyrans are flavonoids, a group of plant secondary metabolites that were implicated in the regulation of auxin transport (Brown et al., 2001). Likewise, BFA was previously shown to indirectly affect auxin transport by impairing subcellular auxin efflux carrier cycling and positioning (Geldner et al., 2001, 2003). Identification of three known auxin transport inhibitors, BFA, and three flavonoids from this screen suggests an essential contribution of auxin transport in *mlo4*- and *mlo11*-conditioned root curling. Owing to the space constraints associated with the microtiter-based compound screen, conclusions on the magnitude of impact of these substances on wild-type roots relative to the mutants were difficult to draw. We therefore focused our study on the effect of the well-characterized auxin transport inhibitor NPA on Col-0 wild-type plants using agar plates. Consistent with a general role of auxin transport in asymmetrical root growth, NPA interfered not only with *mlo4*- and *mlo11*-conditioned root coiling but also with the moderate root curling of Col-0 wild-type plants (Figure 7A). Taken together, these data suggest that MLO4 and MLO11 function upstream of the establishment of auxin distribution patterns and/or auxin transport.

PIN2 plays an essential role in the basipetal transport of auxin to the elongation zone and has been shown to regulate the asymmetrical root growth under gravity stimuli (Chen et al., 1998; Rashotte et al., 2000, 2001). Disruption of *MLO4* seems to have a constitutive positive effect on the expression levels of a pPIN2:PIN2-GFP construct (Figure 3; see Supplemental Figure 5 online). Mutation of *PIN2* (*eir1*-1 mutant) caused significantly decreased root curling as a single mutant (Figure 7B), indicating the importance of PIN2 for this asymmetrical growth pattern. The *eir1*-1 *mlo4*-1 double mutant root exhibited the *eir1* phenotype of reduced root curling (Figure 7B), indicating that the root curling phenotype of *mlo4* also depends on a functional PIN2.

Differential auxin responsiveness is often observed by following auxin-induced reporters in the asymmetrical growth of gravitropism and phototropism (Rashotte et al., 2001; Friml et al., 2002; Paciorek et al., 2005). The involvement of auxin in root curling suggests that the primary vertical stimuli from gravity and light may be interpreted and the response is manifested through asymmetric auxin distribution or signaling in the root tip and/or elongation zone. To examine whether asymmetric auxin-dependent gene expression occurs during root curling, we examined transgenic seedlings expressing the auxin-inducible synthetic *DR5rev:GFP* reporter (Ottenschläger et al., 2003) on horizontal surfaces. In a population of 400 etiolated seedlings, >65% exhibited differential distribution of the GFP-based auxin reporter. Representatives of the four specific types of differential GFP distribution observed at the root tip are shown in Figures 8A to 8D. Regardless of the handedness of root growth, roots with a relatively higher amount of *DR5*-regulated *GFP* expression on the concave side were more prevalent than roots with a *GFP* expression on the convex side. A relatively higher amount of auxin at the concave side of roots was observed during gravity responses as well, and others concluded that this differential auxin distribution drives the orientation of root tip growth (Rashotte et al., 2001; Paciorek et al., 2005). Considering that the steady state level of GFP requires time for biosynthesis upon increase of local auxin concentrations and time for degradation when the auxin level decreases, the observed *DR5*-driven GFP pattern is unlikely to reflect the real-time dynamics of auxin redistribution. To explain the unexpected 19.5% (sum of types shown in Figures 8C and 8D) root tips showing more GFP fluorescence at the convex side of curling roots, we speculate that the GFP signal in these roots represents the auxin

Figure 6. (continued).

The MLO4-MLO2 chimeras (**[A]** to **[P]**) were fused with a C-terminal GFP, and expression in transgenic lines was controlled by the *MLO4* promoter. Black-colored fragments were from MLO4; dark-gray fragments were from MLO2, and light-gray boxes represent transmembrane domains. For each chimera, 20 to 40 light-grown T2 seedlings of six independent transgenic lines were tested for the ability to rescue the *mlo4*-1 phenotype, measured as root span, using Col-0 wild-type and *mlo4*-1 plants on the same plate (minimal medium, 1% sucrose) as controls. Columns indicate the average, and error bars represent SD. Asterisks indicate a statistically significant ($P < 0.05$) difference in comparison to *mlo4* but no significant difference from Col-0 (evidence for full complementation), while the # symbol indicates a statistically significant difference in comparison to both *mlo4* and Col-0 (evidence for partial complementation) according to Bonferroni's multiple comparison test.

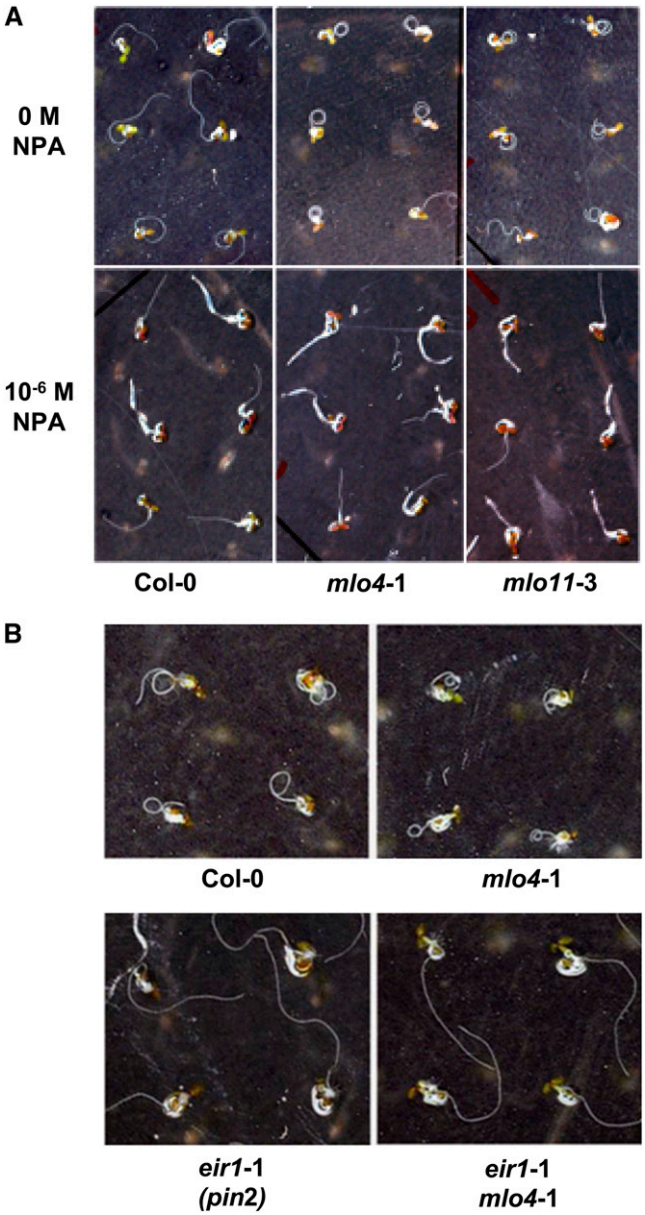

Figure 7. Root Growth Phenotypes of the Wild Type, *mlo4*, and *mlo11* Mutants Depend on Auxin Transport.

(A) Seedlings of the indicated genotypes were grown on horizontal plates (minimal medium, 1% sucrose) under constant light for 5 d, with or without the auxin transport inhibitor NPA (1 μM). Photographs were taken from the bottom. Shown are data from one exemplary replicate; the experiment was repeated twice, yielding similar results.

(B) Seedlings of the indicated genotypes were grown on horizontal plates (minimal medium, 1% sucrose) under constant light for 5 d. Photographs were taken from the bottom. Shown are data from one exemplary replicate; the experiment was repeated twice yielding similar results.

[See online article for color version of this figure.]

distribution pattern established prior to a change in growth direction. Our data demonstrate that lateral auxin asymmetry accompanies naturally occurring asymmetrical root growth.

Since asymmetrical root growth in wild-type plants correlated with characteristic auxin distribution patterns at the root tip, we compared the pattern of auxin-induced gene expression, as an indirect measure of auxin distribution, in wild-type and *mlo4* mutant plants. Compared with the Col-0 wild type, we observed a broader yet symmetrical distribution of *DR5* promoter-regulated *GFP* expression in the root tips of horizontally grown (curling) *mlo4*-3 mutant plants (Figures 8E and 8F). This pattern is reminiscent of *DR5* promoter-driven *GFP* expression in the root tip of the *mdr1/abcb19* mutant, which is defective in an auxin transporter-associated ABC transporter (Lewis et al., 2007). Vertically grown roots of *mdr1/abcb19* seedlings exhibit sporadic root curvature and reduced acropetal auxin transport (Lewis et al., 2007; Wu et al., 2007). In Col-0 and *mlo4*-3 root tips grown vertically on minimal medium, the *DR5*:*GFP* expression pattern was similar to the one observed in Col-0 seedlings grown horizontally. However, accumulation of the GFP signal in cells of the quiescent center was always observed in Col-0 root tips, whereas it was consistently reduced in *mlo4*-3 root tips (Figures 8G and 8H). Notably, these differences in *DR5*:GFP pattern and accumulation were not seen in roots of *mlo4*-3 and wild-type plants vertically grown on MS medium (see Supplemental Figures 10A and 10B online), indicating that the observed effects are not simply due to variation in transgene expression in the two lines but are conditional on the growth direction and medium composition. Taken together, these findings suggest that moderately altered auxin allocation in the root tip might either be the cause for or a consequence of *mlo4*-conditioned asymmetrical root growth.

To further assess the role of auxin in root coiling, we determined basipetal and acropetal auxin transport in mechanically nonstimulated wild type and *mlo4*-4 mutant roots. We observed a minor (1.5-fold) but statistically significant difference in basipetal auxin transport from the root tip into the elongation zone and beyond between Col-0 wild-type and *mlo4*-4 mutant plants (Figure 9A). However, acropetal auxin transport in roots of *mlo4*-4 was strongly (eightfold) increased compared with Col-0 wild-type plants (Figure 9B). Notably, *mlo4* and *mlo11* mutant seedlings exhibited wild-type-like root growth inhibition in response to the exogenous application of the synthetic auxin analogs 2,4-D and naphthalene acetic acid (see Supplemental Figure 11 online). We conclude that altered auxin distribution at the root tip is associated with the enhanced curling of the *mlo4* mutant, which is possibly a consequence of mildly enhanced basipetal and strongly increased acropetal auxin transport.

MLO4-GFP Localizes to the Plasma Membrane and Endomembranes

The altered PIN1 levels (Figure 3), the requirement of auxin transport for root curling (Figure 7), the aberrant *DR5:GFP* expression pattern (Figure 8), and the increased acropetal and basipetal auxin transport (Figure 9B) in *mlo4* mutants suggest an involvement of MLO4 in auxin-related processes. Several proteins involved in polar auxin transport/distribution are known to

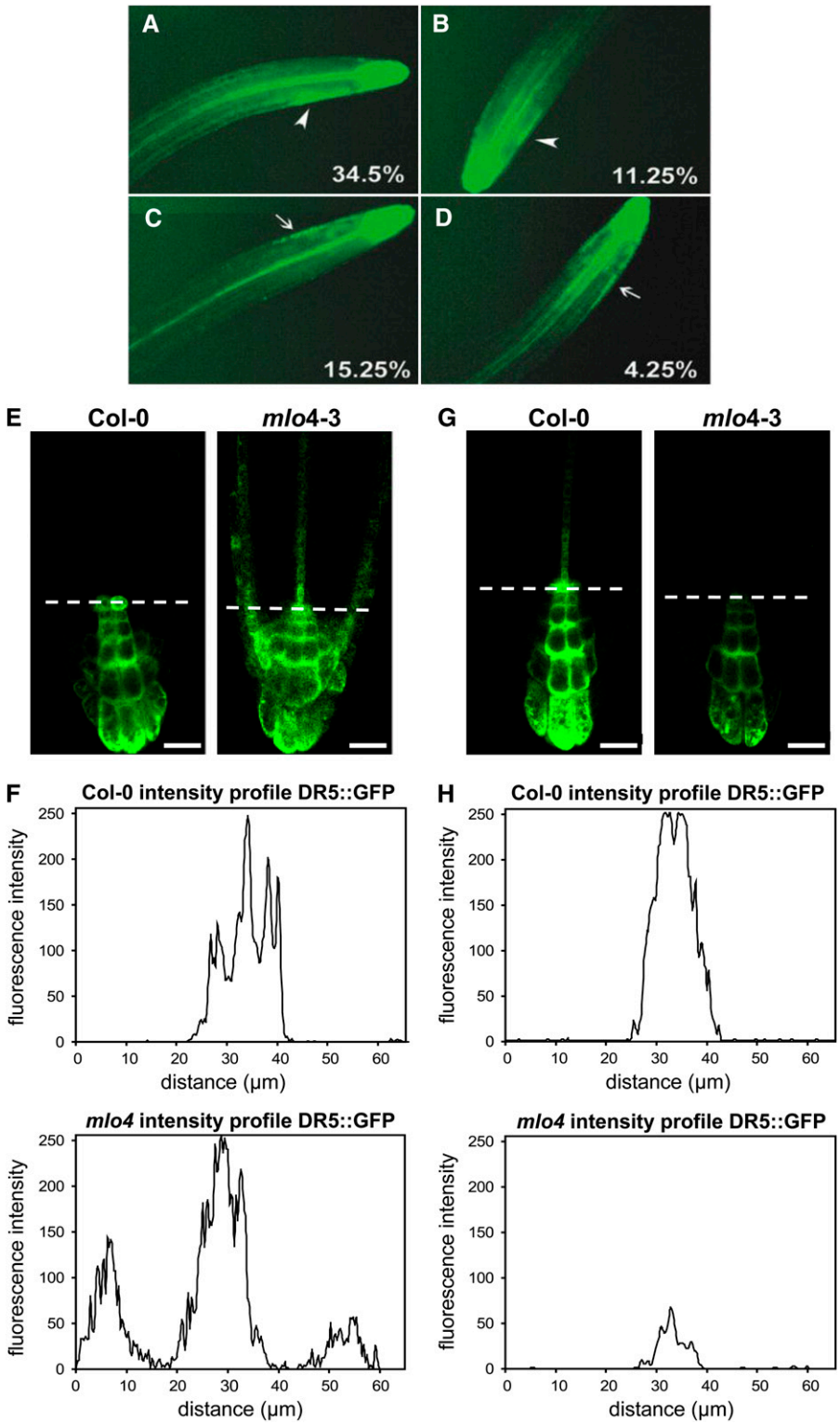

Figure 8. Horizontal Root Curvature and Differential DR5rev:GFP Signal at the Root Tip Region.

(A) and **(C)** Representative epifluorescence micrographs of roots curling clockwise with relatively more *DR5rev:GFP*-derived fluorescent signal at the concave **(A)** or convex **(C)** side.

(B) and **(D)** Representative epifluorescence micrographs of roots curling counterclockwise with relatively more *DR5rev:GFP*-derived fluorescent signal

exhibit asymmetrical subcellular localization (Swarup et al., 2001; Wisniewska et al., 2006; Titapiwatanakun et al., 2009). To determine whether MLO4 also exhibits polarized subcellular localization, we imaged *Arabidopsis* cells expressing the functional MLO4-GFP fusion protein (Figure 6A) under control of the *MLO4* 5′ regulatory sequences in the *mlo4*-1 mutant background. We detected the MLO4-GFP fusion protein at the cell periphery in cells of the root cap, epidermis, and cortex (Figure 10A), consistent with both the gene expression profiles of these root cell types (see Supplemental Figure 12 online) and our previous promoter-GUS fusion studies (Chen et al., 2006). This expression pattern is reminiscent of *PIN2* but distinct from the *PIN1* gene (see Supplemental Figure 12 online; Birnbaum et al., 2003). Confocal imaging of MLO4-GFP in intact roots and root cross sections did not reveal evidence for a potential baso-apical or lateral polarization of the fusion protein (Figures 10A and 10B). Besides localization at the cell periphery, we also observed a prominent intracellular MLO4-GFP pool that largely colocalized with the FM4-64 membrane dye, indicating that the fusion protein is likely subject to continuous cycling between the plasma membrane and endomembrane compartments (Figure 10C). Lack of detectable GFP fluorescence in the nucleus suggests that the majority of the intracellular GFP signal does not result from cytoplasmically localized MLO4-GFP degradation fragments. Cotreatment with FM4-64 and the vesicle trafficking inhibitor BFA led to accumulation of the majority of the intracellular MLO4-GFP signal in spherical intracellular compartments that resemble the previously described Brefeldin or BFA bodies (Orci et al., 1993; Geldner et al., 2001), further supporting that the MLO4-GFP fusion protein is subject to cycling within the endomembrane system (Figure 10D). Similar results were obtained upon coaddition (together with FM4-64 and BFA) of the translation inhibitor cycloheximide, suggesting that it is preexisting and not de novo biosynthesized MLO4-GFP protein that accumulates in the BFA compartments (Geldner et al., 2001). Plasmolysis resulted in retraction of the GFP signal from the cell periphery and visualized fluorescent cell wall–plasma membrane connections (Hechtian strands), corroborating authentic plasma membrane localization of the MLO4-GFP fusion protein (Figure 10E, arrowhead). Taken together, our analysis indicates plasma membrane- and endomembrane-associated MLO4-GFP pools as well as steady endocytotic cycling of the fusion protein, which is reminiscent of the cycling of PIN auxin efflux carriers (Geldner et al., 2001).

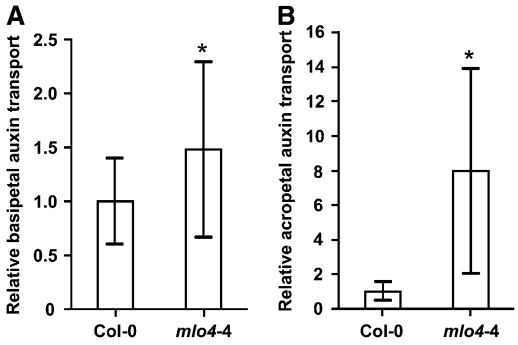

Figure 9. The *mlo4*-4 Mutant Shows Increased Relative Acropetal and Basipetal Auxin Transport Compared with the Wild Type.

Basipetal **(A)** and acropetal **(B)** auxin transport were measured by applying ^{3}H-IAA to the root apex and to the root-shoot junction, respectively. The amount of radioactivity was determined in distal segments of the roots at 5 to 7 h (basipetal transport) or 18 h (acropetal transport) after application of the radiolabeled synthetic auxin. For basipetal auxin transport, data presented are pooled results (obtained in three independent experiments) from 50 wild-type (Col-0) and 24 *mlo4*-4 seedlings. In the case of acropetal transport, three independent assays were performed, and a similar pattern was observed in each experiment. Data were pooled from two independent experiments involving 34 wild-type (Col-0) and 20 *mlo4*-4 seedlings. Data are shown relative to the Col-0 wild type (set as 1). Columns indicate the mean, and error bars represent SD. Asterisks indicate a statistically significant ($P < 0.05$) difference in comparison to Col-0 according to a Student's *t* test.

DISCUSSION

As in the case of root skewing (Rutherford and Masson, 1996), the extent of root curling is subject to natural genetic variation among *Arabidopsis* ecotypes (see Supplemental Figure 2 online), providing an additional example of genetically determined developmental plasticity within a plant species. A continuum of *Arabidopsis* mutants display aberrant root skewing, waving, and/or curling phenotypes (e.g., Okada and Shimura, 1990; Garbers et al., 1996; Rutherford and Masson, 1996; Mullen et al., 1998; Ferrari et al., 2000; Furutani et al., 2000; Yuen et al., 2003; Santner and Watson, 2006; Korolev et al., 2007; Fortunati et al., 2008; Pandey et al., 2008; reviewed in Migliaccio et al., 2009). Consistent with a role for polar auxin transport in tropic organ curvature, several of these mutants are defective in genes

Figure 8. (continued).

at the concave **(B)** or convex **(D)** side. Seedlings were grown horizontally on cover slips overlaid with solidified minimal medium (1% sucrose) for 3 d under darkness before examining. Arrowheads point to stronger *DR5rev:GFP*-derived fluorescent signal at the concave side of curling roots. Arrows point to stronger *DR5rev:GFP*-derived fluorescent signal at the convex side of curling roots. Numbers (bottom right of each image) indicate the frequency of each type of roots among a total population of 400 seedlings examined in two separate experiments.

(E) to **(H)** Representative fluorescence micrographs (confocal sections; **[E]** and **[G]**) of wild-type (Col-0) or *mlo4*-3 mutant plants expressing the *DR5rev:GFP* auxin sensor. Six-day-old seedlings were grown horizontally (**[E]**; i.e., *mlo4*-3 roots exhibit the root curling phenotype) or vertically **(G)** on minimal medium (0.25% sucrose, 12-h light/dark cycle). Information about the fluorescence intensities was extracted from the confocal images along the dotted white line using the Zeiss AIM imaging software and plotted as a function of the distance for horizontally grown **(F)** and vertically grown **(H)** roots of the two genotypes. Shown are representative images with corresponding graphs from one series of experiments. This analysis was repeated twice with similar results. Bars = 20 μm.

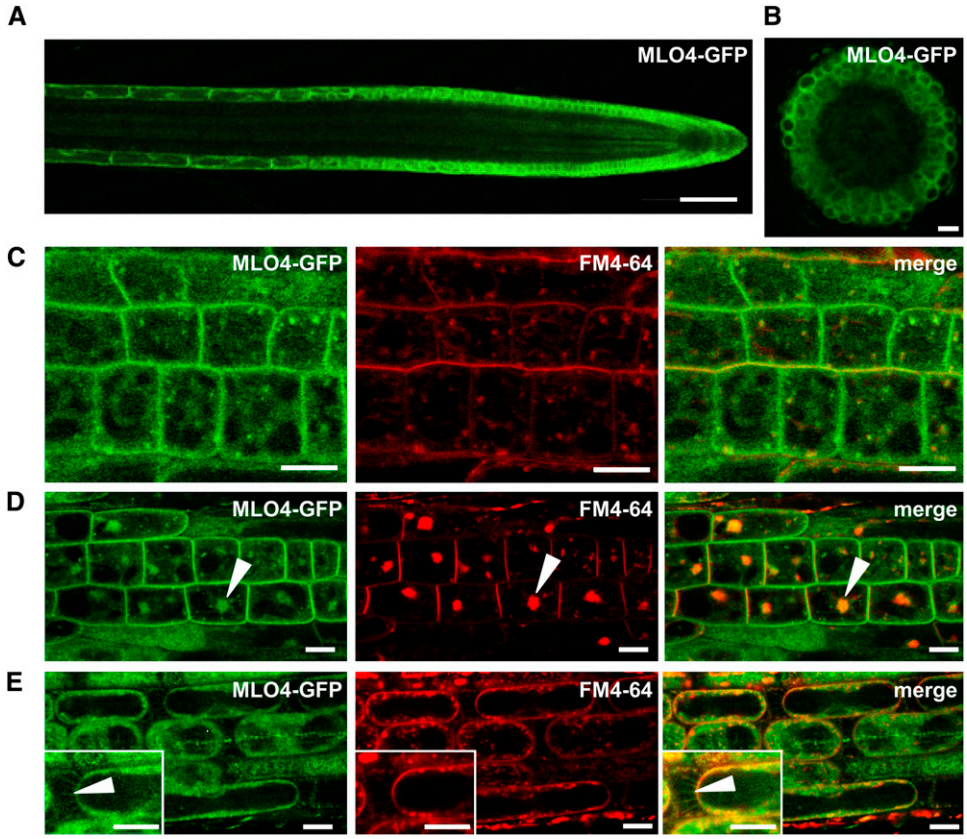

Figure 10. Subcellular Localization of MLO4-GFP.

(A) and **(B)** Fluorescence micrographs (confocal sections) of *Arabidopsis* primary roots expressing MLO4-GFP under transcriptional control of the *MLO4* promoter. Seedlings were grown for 6 d vertically on MS medium (12-h light/dark cycle) prior treatment and/or observation. Longitudinal view **(A)** and cross section through the division zone **(B)**.

(C) Epidermal cells in the division zone showing GFP fluorescence at FM4-64–stained intracellular spots.

(D) Epidermal cells in the division zone treated with BFA and costained with FM4-64 for 2 h. The arrowheads mark a prominent BFA compartment.

(E) Epidermal cells in the elongation zone plasmolyzed with 350 mM mannitol. Insets show magnification of a cell with Hechtian strands (arrowheads). Bars = 100 μm in **(A)**, 20 μm in **(B)**, and 10 μm in **(C)** to **(E)**. Shown are data from one replicate; the experiments were repeated twice, yielding similar results.

encoding components of the auxin biosynthesis/transport pathway, such as *trp2*, *trp3*, *trp5*, *aux1*, and *pin2* (Okada and Shimura, 1990; Rutherford et al., 1998; Piconese et al., 2003). One of the most curious phenotypes is of the *Arabidopsis rcn1* mutant that lacks one out of three phosphatase 2A regulatory A subunits. *rcn1* roots curl more than the wild type in the presence of the auxin transport inhibitor NPA but less than the wild type in the absence of NPA (Garbers et al., 1996). The mutant has enhanced auxin transport that can be reversed to wild-type levels by treatment with NPA (Rashotte et al., 2001), consistent with the root curling phenotype of *rcn1* plants.

The microtubular cytoskeleton is a critical determinant in the axial directionality of organ expansion. The handedness of organ curvature is dictated by an endogenous default structural asymmetry that, at the molecular level, is based on the spatial arrangement of transverse cortical microtubular arrays. Consequently, these arrays shape the arrangement of cellulose microfibrils, thus translating into a preferential directionality of anisotropic organ growth (Furutani et al., 2000; Thitamadee et al., 2002). Consistently, mutants affected in components of the microtubular cytoskeleton, such as *map70*-5, *spr1*, *spr2*, *tua*, *tub*, and *wvd2*, exhibit alterations in the handedness of root skewing (Furutani et al., 2000; Thitamadee et al., 2002; Ishida et al., 2007; Korolev et al., 2007; Perrin et al., 2007).

The most dramatic root curling phenotype described to date is displayed by null alleles of the *MLO4* and *MLO11* genes in the Col-0 ecotype (Figure 1; cf. Supplemental Figure 2 and cited literature). The dramatic root coiling of recessive *mlo4* and *mlo11* mutants requires a tactile stimulus (Figure 1C), is dependent on light and nutrients (Figure 4), and requires an intact auxin transport machinery (Figures 4 and 7) but is independent of medium sucrose content (see Supplemental Figures 2B and 2C online) and is not associated with aberrant gravitropic responses (see Supplemental Figure 6 online). Additionally, *mlo4* and *mlo11* roots are morphologically indistinguishable from wild-type roots, do not show altered cell file arrangement or identity (see

Supplemental Figure 4 online), and do not exhibit altered responsiveness to exogenous application of synthetic auxins (see Supplemental Figure 11 online). Consistent with the hypothesis that root curling, waving, and skewing are mechanistically interconnected (Simmons et al., 1995), *mlo4* and, in part, *mlo11* mutants also exhibited aberrant root waving and root skewing patterns (Figures 1D, 1E, and 2D). Thigmotropic reorientation of root growth directionality involves interplay between the touch and gravity sensing/response systems (Massa and Gilroy, 2003a). It was suggested that both cellular systems share common mechanosensing/transduction elements and crosstalk (Fasano et al., 2002) that might, at least in part, involve a contribution of auxin. This explains why the thigmomorphogenetic defect of *mlo4* and *mlo11* mutants requires intact auxin transport machinery and correlates with an altered auxin distribution pattern (Figure 8) possibly as a result of altered synthesis, transport (Figure 9), and metabolism. The light dependency of *mlo4*-conditioned root curling suggests interplay between light signaling and auxin transport and/or signaling, which is consistent with previous results suggesting crosstalk between light and auxin (Jensen et al., 1998; Rashotte et al., 2003; Cluis et al., 2004).

In wild-type plants, contact of root tips with physical barriers gives rise to unpredictable alternation of growth direction (Figure 1B). By contrast, roots of *mlo4* and *mlo11* mutant plants, once mechanostimulated, initiate genetically predefined and stable growth direction, resulting in curling (Figures 1B and 1C). We speculate that *mlo4* and *mlo11* mutants are defective in resetting the cellular machinery for subsequent perception or interpretation of growth-determining exogenous stimuli, such as touch and/or gravity. In fact, wild-type plants exhibit constant gravitropic resetting of the root tip in response to touch stimulation from encountered physical barriers (Massa and Gilroy, 2003a; Weerasinghe et al., in press). At the molecular level, this reset machinery may comprise plasma membrane–localized mechanosensors and/or ion channels and possibly include heptahelical MLO proteins for which currently there is no known biochemical function.

In an ecophysiological context, root architecture is vital to physically support the growing shoot and to maximize nutrient and water access in the typically nutrient- and water-poor environment of soil substrates. Spiral root growth (manifested as curling on a hard surface) is a morphogenetic process thought to allow roots to penetrate soil, to support circumnavigation of barriers along the main growth trajectory, to advance the establishment of contact to beneficial (growth-promoting) microorganisms, and to offer increased structural support of aerial organs. It presumably also maximizes the exploration of nutrient pools by locally increasing root tissue density within nutrient patches. Simulation of plant growth success for three different degrees of root curling is consistent with the latter concept (see Supplemental Figure 13 online). Besides nutrient and water gradients, positive gravitropism, negative thigmotropism, and root circumnutation are further driving forces decisively shaping root growth patterns. To some extent, the touch-induced root curling pattern of *mlo4* and *mlo11* mutant plants is reminiscent of plant organ circumnutation (Minorsky, 2003). It was suggested that root waving and curling are essentially the consequence of circumnutation, though this view is under debate (Simmons et al., 1995; reviewed in Migliaccio and Piconese, 2001; Oliva and Dunand, 2007). Regardless of the outcome of this debate, in contrast with genuine nutatory organ movements, the anisotropic root growth pattern of *mlo4* and *mlo11* mutant plants is not triggered spontaneously but requires a tactile stimulus. This suggests that these mutants do not show authentic circumnutation but are rather defective in part of the touch-response machinery (see above).

We conclude that MLO4 and MLO11 function as rheostats of root thigmomorphogenesis, representing novel genetically defined, regulatory components of this phenomenon. Like *Arabidopsis* MLO2, MLO6, and MLO12, modulators of antifungal defenses (Consonni et al., 2006), MLO4 and MLO11 reside in a discrete phylogenetic clade of the MLO family (Devoto et al., 2003) and operate in a common physiological process. However, unlike MLO2, MLO6, and MLO12, which function in part redundantly, our genetic data indicate that MLO4 and MLO11 cofunction as regulatory components since *mlo4* and *mlo11* single mutants both exhibit a similar (though not identical) defect in root thigmomorphogenesis (Figures 2A to 2C) that is not further exaggerated in *mlo4 mlo11* double mutants (Figure 2C). Notably, the third member of the *MLO4*/*MLO11*/*MLO14* phylogenetic clade, *MLO14*, does not appear to contribute to this phenomenon since we observed no aberrant root growth pattern in the *mlo14* single mutant and no epistatic effects of *mlo14* on the phenotype of *mlo4* and *mlo11* mutant alleles (Figures 1D, 1E, and 2A to 2D). It would be interesting to learn whether the variability in root curling among *Arabidopsis* ecotypes (see Supplemental Figure 2 online) results, at least in part, from natural genetic variation in *MLO* gene structure and/or expression levels.

Cofunctionality of two sequence-related genes in a common physiological process can be best rationalized by the formation of a heterooligomeric complex of MLO4 and MLO11. Initial evidence for the homooligomerization of MLO proteins results from previous Förster/fluorescence resonance energy transfer experiments demonstrating low levels of energy transfer between yellow fluorescent protein– and cyan fluorescent protein–tagged variants of the barley MLO protein (Elliott et al., 2005). In this scenario, where MLO4 and MLO11 form a heterooligomeric protein assembly, lack of either component (such as in *mlo4* or *mlo11* mutants) would cause identical phenotypes owing to a qualitatively similar impairment of the functional polypeptide complex. The apparent discrepancy between the suggested model and the slight differences in the *mlo4* and *mlo11* root growth patterns (Figure 2A) can be best explained by assuming residual, although qualitatively different, activities of MLO11 and MLO4 homooligomeric protein complexes in *mlo4* and *mlo11* mutants, respectively. It is also possible that loss of either MLO4 or MLO11 would create respective MLO11 or MLO4 homodimers that confer different neomorphic effects. Functionally distinct heterooligomeric protein complexes may likewise account for the observed unequal genetic redundancy of *MLO2*, *MLO6*, and *MLO12* in the context of modulating antifungal defense (Consonni et al., 2006). The formation of heterooligomeric polypeptide assemblies could thus represent a universal feature of MLO proteins. Extensive biochemical work will be required to provide unequivocal experimental evidence for the in planta existence of the proposed heterooligomeric complexes. It will

also be intriguing to learn whether additional polypeptides associate with the hypothesized MLO heterooligomers.

Owing to the topological resemblance of fungal and metazoan GPCRs, MLO proteins were suggested to represent plant surface receptors that may transduce signals via the heterotrimeric G-protein complex (Devoto et al., 1999). Pharmacological and genetic experiments based on the application of G-protein activators and the expression of constitutive active and dominant negative Gα variants in barley epidermal cells did not reveal any evidence for a contribution of heterotrimeric G-protein(s) in MLO-regulated antifungal defense (Kim et al., 2002). Likewise, despite a general modulation of root coiling patterns by the gene encoding the Gβ subunit (Figure 5), genetic analysis also does not support a function of *Arabidopsis* MLO4 and MLO11 as GPCRs in the context of thigmomorphogenesis. Taken together, the data obtained in barley and *Arabidopsis* suggest that the biochemical function of MLO proteins is unrelated to the role of canonical GPCRs. While the findings do not per se exclude a potential role for MLO polypeptides as cell surface receptors, they challenge a cytoplasmic transduction cascade via the heterotrimeric G-protein complex. It also remains possible that MLO proteins exert a primary biochemical function that is distinct from ligand binding and signal transduction.

Previous studies revealed that *Triticum aestivum MLO*-B1, one of the three hexaploid wheat orthologs of barley *Mlo*, fully complements powdery mildew resistance of barley *mlo* mutants, suggesting that the closely related monocot ortholog is functionally equivalent to barley *Mlo* (Elliott et al., 2002, 2005). Surprisingly, domain swap experiments between the two orthologous and highly sequence-related genes showed that chimeric proteins that harbor cytoplasmic domains of the respective counterpart are only partially functional, suggesting cooperative loop–loop interplay either within or between MLO polypeptides (Elliott et al., 2005). In this study, we performed domain-swap experiments between two paralogous *Arabidopsis MLO* members, *MLO2* and *MLO4*, and tested functional specificity of the resulting chimeras in the context of controlling root thigmomorphogenesis. We focused on two regions of the heptahelical proteins that are known to be most divergent: the first extracellular loop and the cytoplasmic C terminus (Devoto et al., 2003). Though potential variation in transgene expression, protein stability, and/or subcellular localization of some chimeras may limit the interpretation of the data, our results suggest that MLO paralogs have a functional identity (Figures 6A and 6B). The findings further indicate that sequence characteristics of the first extracellular loop are dispensable for functional specificity, whereas the C terminus is necessary but not sufficient to confer functional specificity (Figures 6C to 6P). The latter discovery corroborates previous findings demonstrating that both identity and integrity of the cytoplasmic C terminus are critical for MLO functionality and that loop–loop cooperativity is decisive for MLO activity (Elliott et al., 2005). It is intriguing that four Cys residues in the extracellular loops, which are invariant throughout the MLO family, are required for MLO function (Elliott et al., 2005), although at least the sequence context in which three of them are imbedded is irrelevant (Figure 6K). This finding supports the notion that the four Cys residues mainly serve a structural role, most likely by generating two disulphide bridges that stabilize a higher order structure of MLO proteins and/or their homo- and/or heterooligomeric complexes.

Intriguingly, all substances with known biological activity identified in our screen for compounds that interfere with *mlo4*-conditioned root curling directly or indirectly affect auxin transport (see Supplemental Figure 9 online). This finding suggests that polar auxin transport is indeed the primary physiological process that is required for appropriate thigmomorphogenesis. However, we do not rule out other pathways that also contribute to this phenomenon but are either less or not amenable to pharmacological interference. Our data further indicate that the enhanced root curling in *mlo4* is accompanied by subtle changes in auxin-induced gene expression patterns at the root tip (Figure 8) together with altered expression of the auxin efflux carrier fusion proteins PIN2-GFP (see Supplemental Figure 5 online), PIN1-GFP (Figure 3), and enhanced acropetal auxin transport (Figure 9B). Given that the biochemical functions of MLO proteins remain enigmatic, it is currently unclear how heptahelical MLO proteins connect to the root auxin transport/distribution machinery. Unlike proteins directly mediating auxin transport, such as members of the PIN family, MLO4 does not exhibit any obvious subcellular polarization (Figures 10A to 10D).

Although inhibition of basipetal indole-3-acetic acid (IAA) transport by NPA treatment or the *eir1/pin2* mutation abolishes root curling in wild-type and *mlo4/mlo11* mutants, we were able to detect only small changes in root basipetal IAA transport. In comparison, the sporadic spontaneous root curvature and enhanced root waving in the *mdr1/abcb19* mutant, previously shown to have wild-type levels of root basipetal transport, but reduced root acropetal transport, suggests a complex interplay between the two polar auxin transport streams that control mechanically directed root orientation (Lewis et al., 2007; Wu et al., 2007). In addition, the observation that acropetal auxin transport in the *mlo4* mutant was much higher than the wild type while the auxin-induced gene expression patterns were only subtly changed indicates feedback mechanisms between auxin synthesis, movement, response, and breakdown.

METHODS

Plant Materials

The *MLO4* (At1g11000) T-DNA insertions lines *mlo4*-1 (CSH P33B2; Wassilewskija-0 [Ws-0] background), *mlo4*-3 (GABI-KAT_23A10; Col-0 background), and *mlo4*-4 (SAIL_266_C02; Col-0 background), the *MLO11* (At5g53760) T-DNA insertions lines *mlo11*-3 (SALK_076336; Col-0 background) and *mlo11*-4 (SALK_074202; Col-0 background), and the *MLO14* (At1g26700) T-DNA insertion lines *mlo14*-6 (SALK_000216; Col-0 background) and *mlo14*-7 (SALK_046347; Col-0 background) were isolated and confirmed by PCR-based approaches. Primers used are listed in the Supplemental Methods online. The *mlo4*-1 mutant in the Ws-0 background was crossed with Col-0 and homozygous *mlo4* F2 progeny used in the experiments with this *mlo4* allele. The *agb1*-2 and *gpa1*-4 mutants were described previously (Ullah et al., 2001, 2003; Jones et al., 2003). The *Arabidopsis thaliana* mutants *adg1*-1 (Vitha et al., 2000), *pgm1*-1 (Vitha et al., 2000), and *eir1*-1 (Luschnig et al., 1998) as well as a transgenic line expressing *DR5rev:GFP* were obtained from the ABRC (Ohio State University). The *Arabidopsis* mutant *mdr1*-100, (Lin and Wang, 2005) was obtained from Haiyang Wang (Boyce Thompson

Institute), and the *tua4*^{M268I} and *tua4*$^{S178\Delta}$ mutants (Ishida et al., 2007) were provided by Takashi Hashimoto (Nara Institute of Science and Technology, Takayama, Japan). Heterozygous *mlo4*-1 and *mlo11*-3 plants were the F1 plants resulting from crossing wild-type Col-0 plants to *mlo4*-1 and *mlo11*-3 homozygous plants. The double mutants *mlo4*-1 *mlo11*-3, *mlo4*-4 *mlo11*-4, *mlo11*-3 *mlo14*-6, *mlo11*-4 *mlo14*-7, *mlo4*-1 *agb1*-2, *mlo4*-1 *gpa1*-4, *mlo11*-4 *agb1*-2, and *mlo11-4 gpa1*-3 as well as the triple mutant *mlo4*-4 *mlo11*-4 *mlo14*-7 were generated by performing crosses and genotyping the resulting F2 progeny by PCR-based approaches. To generate the *mlo4*-1 *eir1*-1 double mutant, *eir1*-1 was crossed with *mlo4*-1, and homozygous *eir1*-1 mutant seedlings among the F2 population were identified by a straight root phenotype on horizontal plates. The resulting homozygous *mlo4*-1 progeny were detected using PCR-based genotyping. Transgenic lines expressing *pPIN1:PIN1-GFP* (Benková et al., 2003), *pPIN2:PIN2-GFP* (Xu and Scheres, 2005), *pSCR:GFP* (Welch et al., 2007), and *DR5rev:GFP* (Friml et al., 2003) were introgressed into the *mlo4*-1 (*pPIN2:PIN2-GFP*) or *mlo4*-3 (other markers) mutant by crossing. Natural variation of root curling phenotypes was accessed by comparatively analyzing *Arabidopsis* accessions Landsberg *erecta* and Col-0 plus a range of additional ecotypes chosen from the core collection maximized for natural genetic diversity that was described by McKhann et al. (2004): Bay-0 (*Arabidopsis* stock center number N954), Bla-1 (N970), Bur-0 (N1028), Ct-1 (N1094), Cvi-0 (N902), Gre-0 (N1210), Kondara (N916), Ms-0 (N905), Nok-1 (N1400), Ri-0 (N1492), Sav-0 (N1514), Sha (N929), Ta-0 (N1548), and Ws-0 (N1602).

Plant Growth Conditions

We used a medium composition similar to the one reported by Mirza (1987). Briefly, sterilized seeds (Turk et al., 2003) were sown on buffered (0.05% MES, pH 5.7) agar (0.5% [w/v] Phyto or Bacto agar; Research Products International) medium containing either 0.25 or 1% sucrose (in this study referred to as minimal medium). This medium mimics the poor nutrient environment of soil conditions and allows rapid growth of primary roots without initiating lateral roots and therefore is suitable for examining root curvature. For some experiments, where indicated, we used MS medium (1× MS, 0.9% [w/v] Phyto agar, and 1% [w/v] sucrose, pH adjusted to 5.8 with NaOH). Samples for comparisons were placed on the same plate to minimize variations owing to exogenous factors. Plates were incubated at 4°C for 2 or 3 d and then transferred to 21 to 22°C, either wrapped with aluminum foil, or placed under a light source. Considering that roots are underground organs, most of our experiments were performed under constant white light of relatively weaker intensity (30 μmol m^{-2} s^{-1}) compared with the light conditions (160 μmol m^{-2} s^{-1}) used by Mirza (1987). Some experiments were performed in a 12-h or 16-h/8-h light/dark cycle (100 μmol m^{-2} s^{-1}), and some experiments were performed in darkness as indicated. Most of the phenotype characterization and quantitation was performed at both the University of North Carolina at Chapel Hill and at the Max-Planck Institute in Cologne. The acropetal auxin transport assays were performed at both the University of North Carolina at Chapel Hill and at Wake Forest University.

Root Curling and Waving/Skewing Assays

Root curling was measured as described by Mirza (1987) under a dissecting microscope: 5 d after germination on minimal medium, plates were scanned, and seedling root span was measured; roots were then pulled out from the medium and lengths of the roots that produced given angles were measured using a ruler. To eliminate differences introduced by different root growth rates between genotypes, we normalized the degree of root curling by the root length. Root span was assessed by measuring the distance from the root tip to the root base on scanned micrographs. Root waving and skewing were determined on plates containing hard minimal medium (0.05% MES, pH 5.7, 0.25% [w/v] sucrose, and 1.5% [w/v] Phyto agar), held vertically for 48 h, then tilted at 45° (waving) or 35° (skewing) for 4 d. Root skewing was quantified based on the angle between a vertical line drawn downwards from the hypocotyl and the root tip. For all assays, plates were sealed with porous tape to prevent ethylene accumulation. Digital images were captured and processed using either ImageJ (http://rsb.info.nih.gov/ij/) or Adobe Photoshop software.

Chemical Genetics Screen

Chemical compound libraries were provided by Mike Robinson from Syngenta, MicroSource Discovery System (The NatProd Collection; Vogt et al., 2005), and AnalytiCon Discovery (Megabolite Natural Product Library, Berlin, Germany). Surface-sterilized seeds were stratified for 2 to 3 d at 4°C. Seedlings were grown in 96-well microtiter plates (NUNC) containing approximately three to four seeds per well on 100 μL minimal medium (buffered [0.05% MES, pH 5.7] agar [0.5% w/v Bacto agar], and 0.25% sucrose). The microtiter plates were incubated at 21°C in a growth chamber (Percival AR-75L) under 12-h light/dark cycles. After 3 d, chemicals dissolved in DMSO were added with a final concentration of 10 ppm or 10 μM for each compound. Root curling phenotypes were scored 4 d later.

Generation of Transgenic Plants Expressing Chimeric Proteins of MLO2 and MLO4

A 1.05-kb DNA fragment covering the 5′ upstream region of *MLO4* before the start codon was amplified from genomic DNA of wild-type *Arabidopsis* of Col-0 ecotype using Phusion enzyme (Finnzymes). Similarly, fragments of *MLO2* and *MLO4* were amplified from cDNA clones of *MLO2* and *MLO4*. Primers used are listed in Supplemental Methods 1 online. Combinations of overlapping PCR fragments were fused by sequential PCR reactions, so that all chimeric genes were formed under the control of the *MLO4* promoter. These PCR products were cloned into the Gateway pENTR/D-TOPO vector (Invitrogen), sequenced, and moved into the Gateway destination binary vector pGWB4 (Nakagawa et al., 2007b) by Gateway LR recombination reactions. All constructs were transformed into *mlo4*-1 plants via floral dip as described by Clough and Bent (1998). The transgenic plants were selected for resistance to kanamycin and hygromycin (marker genes for both resistances are present in pGWB4, ensuring selection of transgenic plants with full-size T-DNAs), and the presence of the corresponding transgene was confirmed by PCR. For each construct, 20 to 40 seedlings of six independent transgenic lines were tested at the T2 generation for root span and compared with wild-type and *mlo4*-1 mutant seedlings. We defined the criteria for complementation of the *mlo4* root curling phenotype as follows: At least three transgenic T2 lines had to exhibit a root span that in statistical analysis is significantly different from the *mlo4* mutant, but undistinguishable from the Col-0 wild type (full complementation), or at least three transgenic T2 lines had to exhibit a root span that in statistical analysis is significantly different from the *mlo4* mutant and from the Col-0 wild type (partial complementation). Representative fluorescence micrographs depicting expression patterns and subcellular localization of some of the chimeric proteins were taken in the T3 generation.

Confocal Microscopy

Roots of seedlings expressing fluorescent reporter constructs grown on either minimal or MS media were stained in a solution of 4.4 μM FM4-64 (Invitrogen) in water for analysis of endocytic events for the time mentioned with the experiments or with 1 μM FM4-64 in water for >10 min as root contrasting agent. For investigation of MLO4-GFP trafficking, seedlings were incubated in 50 μM cycloheximide (Sigma-Aldrich) and/or 50 μM BFA (Invitrogen) for the times indicated in the figure legends.

Subsequently, the roots were investigated by confocal laser scanning microscopy using a Zeiss LSM 510 META-CONFOCOR2 combination setup. A ×40 C-Apochromat water immersion objective (Zeiss) with a numerical aperture of 1.2 was used. GFP was excited with the 488-nm argon laser line, and excitation and emission light were separated by a HTF488 dichroic filter. GFP fluorescence was filtered through a 505- to 530-nm band-pass filter before detection. FM 4-64 was excited by the 543-nm laser line of the helium laser. Excitation and emission light were separated by a 543-nm dichroic filter. FM4-64 fluorescence was filtered by a 650- to 710-nm band-pass filter before detection. For GFP signal quantification, confocal images of roots expressing the fluorescent markers were taken as a consecutive series along the *z* axis. Microscope settings were kept the same for all measurements. To assess differences in signal intensity in an unbiased manner, a maximum intensity projection along the *z* axis was generated of the series of confocal images using the Zeiss LSM imaging software (version 3.2 SP2) and Zeiss LSM image examiner (version 3.1). Subsequently, fluorescence intensities in the projection were analyzed using ImageJ 1.37 (http://rsbweb.nih.gov/ij/). Significance levels of observed differences in fluorescence intensities were assessed with a Student's *t* test.

Basipetal and Acropetal Auxin Transport Assays

Basipetal and acropetal auxin transport measurements were performed in roots of Col-0 wild-type and *mlo4*-4 mutant seedlings as previously described (Lewis and Muday, 2009). Seedlings were grown vertically under long-day conditions (16-h/8-h light/dark cycle; 100 μmol m^{-2} s^{-1}) for 5 d on minimal medium (0.25% sucrose). For each experiment, 10 to 15 seedlings were moved and aligned on a fresh minimal medium plate. For basipetal auxin transport assays, ^{3}H-IAA agar lines (final concentration of 200 nM) were applied to the aligned root tips of the seedling. Plates were incubated vertically in the dark for 5 to 7 h. Subsequently, the first 2 mm of the root tip touching the radioactive agar was discarded and the 5-mm section of the root above the site of cut was assayed for radioactivity by scintillation counting. For acropetal auxin transport assays, ^{3}H-IAA agar lines (final concentration of 200 nM) were applied to the root region just below the root-shoot junction. Plates were inverted upside down and vertically incubated in the dark for 18 h. Subsequently, agar lines were removed, roots straightened (as they would have responded to gravity), and 5-mm sections from the root tip were cut and measured for radioactivity by scintillation counting.

Study of Bending Direction and Differential Auxin Distribution at the Root Tip

To study bending direction and visualize differential auxin distribution in root tips, *DR5rev:GFP* transgenic seedlings (Friml et al., 2003) were grown on cover slides overlaid with a thin layer of solidified root growth minimal medium in a sterile Petri dish placed horizontally under dark for 3 d after incubation at 4°C for 2 or 3 d. GFP and curvature were imaged with an Olympus IX81 microscope.

Statistical Analyses

We performed Bonferroni's multiple comparison test (GraphPad Prism; http://www.graphpad.com/prism/Prism.htm) when analyzing multiple data sets in comparison with a control and employed a two-tailed Student's *t* test with unequal variances when analyzing single data sets in comparison with a control. An F-test was used to comparatively analyze sample variance.

Computer Simulation of Plant Growth Success

We used the software MATLAB 7.3.0 to simulate the growth of roots in matrices containing, at the indicated density, randomly distributed resource spots having a diameter equivalent to the width of the root or in matrices containing randomly distributed resource spots of different sizes at a given density. Three roots of the same length but different in degrees of curling tightness were generated for these tests. Summation of the number of intersections between a resource spot (counted only once) over the length of each root equals an estimate for plant growth success. The original code is provided in Supplemental Figure 13E online and additionally as a text file in Supplemental Methods online.

Accession Numbers

Sequence data from this article can be found in the Arabidopsis Genome Initiative or GenBank/EMBL databases under the following accession numbers: *ACTIN2*, At3g18780; *AGB1*, At4g34460; *GPA1*, At2g26300; *MLO2*, At1g11310; *MLO4*, At1g11000; *MLO11*, At5g53760; *MLO14*, At1g26700; *PIN1*, At1g73590; and *PIN2*, At5g57090.

Supplemental Data

The following materials are available in the online version of this article.

Supplemental Figure 1. Absence of Full-Length Transcripts of *MLO4*, *MLO11*, and *MLO14* in *mlo4*, *mlo11*, and *mlo14* Alleles.

Supplemental Figure 2. Natural Variation and Sucrose Independence of the Root Curling Phenotype.

Supplemental Figure 3. Negative Correlation between Root Curling and Root Span in a Population of Wild-Type Seedlings.

Supplemental Figure 4. *mlo4* Roots Show Unaltered Cell File Organization and No Evidence for Cell File Torsion.

Supplemental Figure 5. Expression Pattern of the Cell Identity Markers PIN1 and PIN2.

Supplemental Figure 6. Roots of Light-Grown *mlo4* and *mlo11* Mutants Exhibit Unaltered Response to a Gravistimulus.

Supplemental Figure 7. *mlo2* Mutant Seedlings Exhibit Wild-Type Root Curling.

Supplemental Figure 8. Protein Accumulation and Subcellular Localization of Chimeric MLO-GFP Proteins.

Supplemental Figure 9. Chemicals Disrupting Auxin Transport or Function Abolish the *mlo4* Root Curling Phenotype.

Supplemental Figure 10. Auxin Distribution at the Root Tip of Vertically Grown *mlo4* Seedlings Is Not Affected on MS Medium.

Supplemental Figure 11. Unaltered Auxin Responsiveness of *mlo4* and *mlo11* Mutants.

Supplemental Figure 12. *PIN2*, but Not *PIN1*, Has a Similar Expression Pattern in Root Cell Files as *MLO4* and *MLO11*.

Supplemental Figure 13. Horizontal Root Curvature Impacts Plant Growth Success.

Supplemental Methods 1. Primers Used in This Study and Matlab Program Used to Generate Data Shown in Supplemental Figure 13D.

ACKNOWLEDGMENTS

This work was supported by grants from the National Institute of General Medical Sciences (GM65989-01), the Department of Energy (DE-FG02-05er15671), and the National Science Foundation (MCB-0209711 and MCB-0723515) to A.M.J.; from the National Research Initiative of the USDA (2006-35304-17311) to G.M.; and from the Deutsche Forschungsgemeinschaft (PA861/6-1; AFGN) and Max-Planck Society to R.P. We thank Jing Yang, Anja Reinstädler, and Shannon Booker for

technical assistance and Haiyang Wang, Takashi Hashimoto, Renze Heidstra, Ben Scheres, and Jiri Friml for providing genetic material as well as Mike Robinson for making available a core set of the Syngenta chemical library.

Received August 18, 2008; revised June 10, 2009; accepted June 24, 2009; published July 14, 2009.

REFERENCES

Benková, E., Michniewicz, M., Sauer, M., Teichmann, T., Seifertová, D., Jürgens, G., and Friml, J. (2003). Local, efflux-dependent auxin gradients as a common module for plant organ formation. Cell **115:** 591–602.

Birnbaum, K., Shasha, D.E., Wang, J.Y., Jung, J.W., Lambert, G.M., Galbraith, D.W., and Benfey, P.N. (2003). A gene expression map of the Arabidopsis root. Science **302:** 1956–1960.

Blancaflor, E.B., Fasano, J.M., and Gilroy, S. (1998). Mapping the functional roles of cap cells in the response of Arabidopsis primary roots to gravity. Plant Physiol. **116:** 213–222.

Braam, J., and Davis, R.W. (1990). Rain-induced, wind-induced, and touch-induced expression of calmodulin and calmodulin-related genes in Arabidopsis. Cell **60:** 357–364.

Brown, D.E., Rashotte, A.M., Murphy, A.S., Normanly, J., Tague, B.W., Peer, W.A., Taiz, L., and Muday, G.K. (2001). Flavonoids act as negative regulators of auxin transport in vivo in Arabidopsis. Plant Physiol. **126:** 524–535.

Buer, C.S., Masle, J., and Wasteneys, G.O. (2000). Growth conditions modulate root-wave phenotypes in Arabidopsis. Plant Cell Physiol. **41:** 1164–1170.

Buer, C.S., and Muday, G.K. (2004). The transparent *testa4* mutation prevents flavonoid synthesis and alters auxin transport and the response of *Arabidopsis* roots to gravity and light. Plant Cell **16:** 1191–1205.

Buer, C.S., Sukumar, P., and Muday, G.K. (2006). Ethylene modulates flavonoid accumulation and gravitropic responses in roots of Arabidopsis. Plant Physiol. **140:** 1384–1396.

Buer, C.S., Wasteneys, G.O., and Masle, J. (2003). Ethylene modulates root-wave responses in Arabidopsis. Plant Physiol. **132:** 1085–1096.

Büschges, R., et al. (1997). The barley *Mlo* gene: A novel control element of plant pathogen resistance. Cell **88:** 695–705.

Chachisvilis, M., Zhang, Y.L., and Frangos, J.A. (2006). G protein-coupled receptors sense fluid shear stress in endothelial cells. Proc. Natl. Acad. Sci. USA **103:** 15463–15468.

Chen, R.J., Hilson, P., Sedbrook, J., Rosen, E., Caspar, T., and Masson, P.H. (1998). The *Arabidopsis thaliana AGRAVITROPIC 1* gene encodes a component of the polar-auxin-transport efflux carrier. Proc. Natl. Acad. Sci. USA **95:** 15112–15117.

Chen, Z., Hartmann, H.A., Wu, M.J., Friedman, E.J., Chen, J.G., Pulley, M., Schulze-Lefert, P., Panstruga, R., and Jones, A.M. (2006). Expression analysis of the *AtMLO* gene family encoding plant-specific seven-transmembrane domain proteins. Plant Mol. Biol. **60:** 583–597.

Clough, S.J., and Bent, A.F. (1998). Floral dip: A simplified method for *Agrobacterium*-mediated transformation of *Arabidopsis thaliana.* Plant J. **16:** 735–743.

Cluis, C.P., Mouchel, C.F., and Hardtke, C.S. (2004). The Arabidopsis transcription factor HY5 integrates light and hormone signaling pathways. Plant J. **38:** 332–347.

Consonni, C., Humphry, M.E., Hartmann, H.A., Livaja, M., Durner, J., Westphal, L., Vogel, J., Lipka, V., Kemmerling, B., Schulze-Lefert, P., Somerville, S.C., and Panstruga, R. (2006). Conserved requirement for a plant host cell protein in powdery mildew pathogenesis. Nat. Genet. **38:** 716–720.

de Dorlodot, S., Forster, B., Pagès, L., Price, A., Tuberosa, R., and Draye, X. (2007). Root system architecture: Opportunities and constraints for genetic improvement of crops. Trends Plant Sci. **12:** 474–481.

Devoto, A., Hartmann, H.A., Piffanelli, P., Elliott, C., Simmons, C., Taramino, G., Goh, C.S., Cohen, F.E., Emerson, B.C., Schulze-Lefert, P., and Panstruga, R. (2003). Molecular phylogeny and evolution of the plant-specific seven-transmembrane MLO family. J. Mol. Evol. **56:** 77–88.

Devoto, A., Piffanelli, P., Nilsson, I., Wallin, E., Panstruga, R., von Heijne, G., and Schulze-Lefert, P. (1999). Topology, subcellular localization, and sequence diversity of the *Mlo* family in plants. J. Biol. Chem. **274:** 34993–35004.

Elliott, C., Müller, J., Miklis, M., Bhat, R.A., Schulze-Lefert, P., and Panstruga, R. (2005). Conserved extracellular cysteine residues and cytoplasmic loop-loop interplay are required for functionality of the heptahelical MLO protein. Biochem. J. **385:** 243–254.

Elliott, C., Zhou, F., Spielmeyer, W., Panstruga, R., and Schulze-Lefert, P. (2002). Functional conservation of wheat and rice *Mlo* orthologs in defense modulation to the powdery mildew fungus. Mol. Plant Microbe Interact. **15:** 1069–1077.

Fasano, J.M., Massa, G.D., and Gilroy, S. (2002). Ionic signaling in plant responses to gravity and touch. J. Plant Growth Regul. **21:** 71–88.

Fasano, J.M., Swanson, S.J., Blancaflor, E.B., Dowd, P.E., Kao, T.-h., and Gilroy, S. (2001). Changes in root cap pH are required for the gravity response of the *Arabidopsis* root. Plant Cell **13:** 907–922.

Ferrari, S., Piconese, S., Tronelli, G., and Migliaccio, T.F. (2000). A new *Arabidopsis thaliana* root gravitropism and chirality mutant. Plant Sci. **158:** 77–85.

Fortunati, A., Piconese, S., Tassone, P., Ferrari, S., and Migliaccio, F. (2008). A new mutant of Arabidopsis disturbed in its roots, right-handed slanting, and gravitropism defines a gene that encodes a heat-shock factor. J. Exp. Bot. **59:** 1363–1374.

Friml, J., Vieten, A., Sauer, M., Weijers, D., Schwarz, H., Hamann, T., Offringa, R., and Jurgens, G. (2003). Efflux-dependent auxin gradients establish the apical-basal axis of Arabidopsis. Nature **426:** 147–153.

Friml, J., Wisniewska, J., Benkova, E., Mendgen, K., and Palme, K. (2002). Lateral relocation of auxin efflux regulator PIN3 mediates tropism in Arabidopsis. Nature **415:** 806–809.

Furutani, I., Watanabe, Y., Prieto, R., Masukawa, M., Suzuki, K., Naoi, K., Thitamadee, S., Shikanai, T., and Hashimoto, T. (2000). The *SPIRAL* genes are required for directional central of cell elongation in *Arabidopsis thaliana.* Development **127:** 4443–4453.

Garbers, C., DeLong, A., Deruere, J., Bernasconi, P., and Soll, D. (1996). A mutation in protein phosphatase 2A regulatory subunit A affects auxin transport in Arabidopsis. EMBO J. **15:** 2115–2124.

Geldner, N., Anders, N., Wolters, H., Keicher, J., Kornberger, W., Müller, P., Delbarre, A., Ueda, T., Nakano, A., and Jürgens, G. (2003). The Arabidopsis GNOM ARF-GEF mediates endosomal recycling, auxin transport, and auxin-dependent plant growth. Cell **112:** 219–230.

Geldner, N., Friml, J., Stierhof, Y.-D., Jürgens, G., and Palme, K. (2001). Auxin transport inhibitors block PIN1 cycling and vesicle trafficking. Nature **413:** 425–428.

Gookin, T., Kim, J., and Assmann, S.M. (2008). Whole proteome identification of plant candidate G-protein coupled receptors in Arabidopsis, rice, and poplar: Computational prediction and in vivo protein coupling. Genome Biol. **9:** R120.

Ishida, T., Kaneko, Y., Iwano, M., and Hashimoto, T. (2007). Helical microtubule arrays in a collection of twisting tubulin mutants of *Arabidopsis thaliana.* Proc. Natl. Acad. Sci. USA **104:** 8544–8549.

Jaffe, M.J., Leopold, A.C., and Staples, R.C. (2002). Thigmo responses in plants and fungi. Am. J. Bot. **89:** 375–382.

Jensen, P.J., Hangarter, R.P., and Estelle, M. (1998). Auxin transport is required for hypocotyl elongation in light-grown but not dark-grown Arabidopsis. Plant Physiol. **116:** 455–462.

Jones, A.M., Ecker, J.R., and Chen, J.G. (2003). A reevaluation of the role of the heterotrimeric G protein in coupling light responses in Arabidopsis. Plant Physiol. **131:** 1623–1627.

Kim, M.C., Panstruga, R., Elliott, C., Müller, J., Devoto, A., Yoon, H.W., Park, H.C., Cho, M.J., and Schulze-Lefert, P. (2002). Calmodulin interacts with MLO protein to regulate defence against mildew in barley. Nature **416:** 447–451.

Knight, M.R., Campbell, A.K., Smith, S.M., and Trewavas, A.J. (1991). Transgenic plant aequorin reports the effects of touch and cold-shock and elicitors on cytoplasmic calcium. Nature **352:** 524–526.

Korolev, A.V., Buschmann, H., Doonan, J.H., and Lloyd, C.W. (2007). AtMAP70-5, a divergent member of the MAP70 family of microtubule-associated proteins, is required for anisotropic cell growth in Arabidopsis. J. Cell Sci. **120:** 2241–2247.

Kumamoto, C.A. (2008). Molecular mechanisms of mechanosensing and their roles in fungal contact sensing. Nat. Rev. Microbiol. **6:** 667–673.

Legué, V., Blancaflor, E., Wymer, C., Perbal, G., Fantin, D., and Gilroy, S. (1997). Cytoplasmic free Ca^{2+} in Arabidopsis roots changes in response to touch but not gravity. Plant Physiol. **114:** 789–800.

Lewis, D.R., Miller, N.D., Splitt, B.L., Wu, G., and Spalding, E.P. (2007). Separating the roles of acropetal and basipetal auxin transport on gravitropism with mutations in two Arabidopsis *multidrug resistance-like* ABC transporter genes. Plant Cell **19:** 1838–1850.

Lewis, D.R., and Muday, G.K. (2009). Measurement of auxin transport in *Arabidopsis thaliana.* Nat. Protocols **4:** 437–451.

Lin, R., and Wang, H. (2005). Two homologous ATP-binding cassette transporter proteins, AtMDR1 and AtPGP1, regulate Arabidopsis photomorphogenesis and root development by mediating polar auxin transport. Plant Physiol. **138:** 949–964.

Luschnig, C., Gaxiola, R.A., Grisafi, P., and Fink, G.R. (1998). EIR1, a root-specific protein involved in auxin transport, is required for gravitropism in *Arabidopsis thaliana.* Genes Dev. **12:** 2175–2187.

Malamy, J. (2005). Intrinsic and environmental response pathways that regulate root system architecture. Plant Cell Environ. **28:** 67–77.

Marchant, A., Kargul, J., May, S.T., Muller, P., Delbarre, A., Perrot-Rechenmann, C., and Bennett, M.J. (1999). AUX1 regulates root gravitropism in Arabidopsis by facilitating auxin uptake within root apical tissues. EMBO J. **18:** 2066–2073.

Massa, G.D., and Gilroy, S. (2003a). Touch modulates gravity sensing to regulate the growth of primary roots of *Arabidopsis thaliana.* Plant J. **33:** 435–445.

Massa, G.D., and Gilroy, S. (2003b). Touch and gravitropic set-point angle interact to modulate gravitropic growth in roots. Adv. Space Res. **31:** 2195–2202.

McKhann, H.I., Camilleri, C., Bérard, A., Bataillon, T., David, J.L., Reboud, X., Le Corre, V., Caloustian, C., Gut, I.G., and Brunel, D. (2004). Nested core collections maximizing genetic diversity in *Arabidopsis thaliana.* Plant J. **38:** 193–202.

Migliaccio, F., Fortunati, A., and Tassonese, P. (2009). Arabidopsis root growth movements and their symmetry. Plant Signal. Behav. **4:** 183–190.

Migliaccio, F., and Piconese, S. (2001). Spiralizations and tropisms in Arabidopsis roots. Trends Plant Sci. **6:** 561–565.

Minorsky, P.V. (2003). The hot and the classic - Circumnutation. Plant Physiol. **132:** 1779–1780.

Mirza, J.I. (1987). The effects of light and gravity on the horizontal curvature of roots of gravitropic and agravitropic *Arabidopsis thaliana* L. Plant Physiol. **83:** 118–120.

Moriyama, E.N., Strope, P.K., Opiyo, S.O., Chen, Z., and Jones, A.M. (2006). Mining the *Arabidopsis thaliana* genome for highly-divergent seven transmembrane receptors. Genome Biol. **7:** R96.

Muday, G., and Rahman, A. (2007). Auxin transport and the integration of gravitropic growth. In Plant Tropisms, S. Gilroy and P. Masson, eds (Blackwell Publishing, Ames, Iowa), pp. 47–78.

Mullen, J.L., Turk, E., Johnson, K., Wolverton, C., Ishikawa, H., Simmons, C., Soll, D., and Evans, M.L. (1998). Root-growth behavior of the Arabidopsis mutant *rgr1* Roles of gravitropism and circumnutation in the waving/coiling phenomenon. Plant Physiol. **118:** 1139–1145.

Nakagawa, T., Kurose, T., Hino, T., Tanaka, K., Kawamukai, M., Niwa, Y., Toyooka, K., Matsuoka, K., Jinbo, T., and Kimura, T. (2007b). Development of series of gateway binary vectors, pGWBs, for realizing efficient construction of fusion genes for plant transformation. J. Biosci. Bioeng. **104:** 34–41.

Nakagawa, Y., et al. (2007a). Arabidopsis plasma membrane protein crucial for Ca^{2+} influx and touch sensing in roots. Proc. Natl. Acad. Sci. USA **104:** 3639–3644.

Negi, S., Ivanchenko, M.G., and Muday, G.K. (2008). Ethylene regulates lateral root formation and auxin transport in *Arabidopsis thaliana.* Plant J. **55:** 175–187.

Okada, K., and Shimura, Y. (1990). Reversible root tip rotation in Arabidopsis seedlings induced by obstacle-touching stimulus. Science **250:** 274–276.

Oliva, M., and Dunand, C. (2007). Waving and skewing: how gravity and the surface of growth media affect root development in Arabidopsis. New Phytol. **176:** 37–43.

Orci, L., Perrelet, A., Ravazzola, M., Wieland, F.T., Schekman, R., and Rothman, J.E. (1993). BFA bodies - A subcompartment of the endoplasmic reticulum. Proc. Natl. Acad. Sci. USA **90:** 11089–11093.

Osmont, K.S., Sibout, R., and Hardtke, C.S. (2007). Hidden branches: Developments in root system architecture. Annu. Rev. Plant Biol. **58:** 93–113.

Ottenschläger, I., Wolff, P., Wolverton, C., Bhalerao, R.P., Sandberg, G., Ishikawa, H., Evans, M., and Palme, K. (2003). Gravity-regulated differential auxin transport from columella to lateral root cap cells. Proc. Natl. Acad. Sci. USA **100:** 2987–2991.

Paciorek, T., Zazimalova, E., Ruthardt, N., Petrasek, J., Stierhof, Y.D., Kleine-Vehn, J., Morris, D.A., Emans, N., Jurgens, G., Geldner, N., and Friml, J. (2005). Auxin inhibits endocytosis and promotes its own efflux from cells. Nature **435:** 1251–1256.

Pandey, S., Monshausen, G.B., Ding, L., and Assmann, S.M. (2008). Regulation of root-wave response by extra large and conventional G proteins in *Arabidopsis thaliana.* Plant J. **55:** 311–322.

Panstruga, R. (2005). Discovery of novel conserved peptide domains by ortholog comparison within plant multi-protein families. Plant Mol. Biol. **59:** 485–500.

Perrin, R.M., Wang, Y., Yuen, C.Y.L., Will, J., and Masson, P.H. (2007). WVD2 is a novel microtubule-associated protein in *Arabidopsis thaliana.* Plant J. **49:** 961–971.

Piconese, S., Tronelli, G., Pippia, P., and Migliaccio, F. (2003). Chiral and non-chiral nutations in Arabidopsis roots grown on the random positioning machine. J. Exp. Bot. **54:** 1909–1918.

Piffanelli, P., Zhou, F., Casais, C., Orme, J., Jarosch, B., Schaffrath, U., Collins, N.C., Panstruga, R., and Schulze-Lefert, P. (2002). The barley MLO modulator of defense and cell death is responsive to biotic and abiotic stress stimuli. Plant Physiol. **129:** 1076–1085.

Rashotte, A.M., Brady, S.R., Reed, R.C., Ante, S.J., and Muday, G.K. (2000). Basipetal auxin transport is required for gravitropism in roots of Arabidopsis. Plant Physiol. **122:** 481–490.

Rashotte, A.M., DeLong, A., and Muday, G.K. (2001). Genetic and chemical reductions in protein phosphatase activity alter auxin transport, gravity response, and lateral root growth. Plant Cell **13:** 1683–1697.

Rashotte, A.M., Poupart, J., Waddell, C.S., and Muday, G.K. (2003). Transport of the two natural auxins, indole-3-butyric acid and indole-3-acetic acid, in Arabidopsis. Plant Physiol. **133:** 761–772.

Rutherford, R., Gallois, P., and Masson, P.H. (1998). Mutations in *Arabidopsis thaliana* genes involved in the tryptophan biosynthesis pathway affect root waving on tilted agar surfaces. Plant J. **16:** 145–154.

Rutherford, R., and Masson, P.H. (1996). *Arabidopsis thaliana sku* mutant seedlings show exaggerated surface-dependent alteration in root growth vector. Plant Physiol. **111:** 987–998.

Sack, F. (1997). Plastids and gravitropic sensing. Planta **203:** S63–S68.

Santner, A.A., and Watson, J.C. (2006). The WAG1 and WAG2 protein kinases negatively regulate root waving in Arabidopsis. Plant J. **45:** 752–764.

Simmons, C., Soll, D., and Migliaccio, F. (1995). Circumnutation and gravitropism cause root waving in *Arabidopsis thaliana.* J. Exp. Bot. **46:** 143–150.

Sistrunk, M.L., Antosiewicz, D.M., Purugganan, M.M., and Bra.am, J. (1994). Arabidopsis *Tch3* encodes a novel Ca^{2+} binding-protein and shows environmentally induced and tissue-specific regulation. Plant Cell **6:** 1553–1565.

Swarup, R., Friml, J., Marchant, A., Ljung, K., Sandberg, G., Palme, K., and Bennett, M. (2001). Localization of the auxin permease AUX1 suggests two functionally distinct hormone transport pathways operate in the Arabidopsis root apex. Genes Dev. **15:** 2648–2653.

Temple, B.R.S., and Jones, A.M. (2007). The plant heterotrimeric G protein complex. Annu. Rev. Plant Biol. **58:** 249–266.

Thitamadee, S., Tuchihara, K., and Hashimoto, T. (2002). Microtubule basis for left-handed helical growth in Arabidopsis. Nature **417:** 193–196.

Titapiwatanakun, B., et al. (2009). ABCB19/PGP19 stabilises PIN1 in membrane microdomains in Arabidopsis. Plant J. **57:** 27–44.

Turk, E.M., Fujioka, S., Seto, H., Shimada, Y., Takatsuto, S., Yoshida, S., Denzel, M.A., Torres, Q.I., and Neff, M.M. (2003). CYP72B1 inactivates brassinosteroid hormones: An intersection between photomorphogenesis and plant steroid signal transduction. Plant Physiol. **133:** 1643–1653.

Ullah, H., Chen, J.G., Temple, B., Boyes, D.C., Alonso, J.M., Davis, K.R., Ecker, J.R., and Jones, A.M. (2003). The beta-subunit of the *Arabidopsis* G protein negatively regulates auxin-induced cell division and affects multiple developmental processes. Plant Cell **15:** 393–409.

Ullah, H., Chen, J.G., Young, J.C., Im, K.H., Sussman, M.R., and Jones, A.M. (2001). Modulation of cell proliferation by heterotrimeric G protein in Arabidopsis. Science **292:** 2066–2069.

Vitha, S., Zhao, L., and Sack, F.D. (2000). Interaction of root gravitropism and phototropism in Arabidopsis wild-type and starchless mutants. Plant Physiol. **122:** 453–462.

Vogt, A., Tamewitz, A., Skoko, J., Sikorski, R.P., Giuliano, K.A., and Lazo, J.S. (2005). The benzo[c]phenanthridine alkaloid, sanguinarine, is a selective, cell-active inhibitor of mitogen-activated protein kinase phosphatase-1. J. Biol. Chem. **280:** 19078–19086.

Weerasinghe, R.R., Swanson, S.J., Okada, S.F., Garrett, M.B., Kim, S-Y., Stacey, G., Boucher, R.C., Gilroy, S., and Jones, A.M. (2009). Touch induces ATP release in Arabidopsis roots that is modulated by the heterotrimeric G protein complex. FEBS Lett (in press).

Welch, D., Hassan, H., Blilou, I., Immink, R., Heidstra, R., and Scheres, B. (2007). Arabidopsis JACKDAW and MAGPIE zinc finger proteins delimit asymmetric cell division and stabilize tissue boundaries by restricting SHORT-ROOT action. Genes Dev. **21:** 2196–2204.

Wisniewska, J., Xu, J., Seifertova, D., Brewer, P.B., Ruzicka, K., Blilou, I., Rouquie, D., Benkova, E., Scheres, B., and Friml, J. (2006). Polar PIN ocalization directs auxin flow in plants. Science **312:** 883.

Wu, G., Lewis, D.R., and Spalding, E.P. (2007). Mutations in *Arabidopsis Multidrug Resistance-Like* ABC transporters separate the roles of acropetal and basipetal auxin transport in lateral root development. Plant Cell **19:** 1826–1837.

Xu, J., and Scheres, B. (2005). Dissection of Arabidopsis ADP-RIBOSYLATION FACTOR 1 function in epidermal cell polarity. Plant Cell **17:** 525–536.

Yuen, C.Y.L., Pearlman, R.S., Silo-Suh, L., Hilson, P., Carroll, K.L., and Masson, P.H. (2003). WVD2 and WDL1 modulate helical organ growth and anisotropic cell expansion in Arabidopsis. Plant Physiol. **131:** 493–506.